HHS Public Access

Author manuscript

J Comp Neurol. Author manuscript; available in PMC 2022 March 01.

Published in final edited form as:

J Comp Neurol. 2021 March ; 529(4): 657–693. doi:10.1002/cne.24975.

Efferent Projections of Vglut2, Foxp2 and Pdyn Parabrachial Neurons in Mice

Dake Huang[1], **Fillan S. Grady**[1], **Lila Peltekian**[1], **Joel C. Geerling**[1,*]

[1]Department of Neurology, University of Iowa

Abstract

The parabrachial nucleus (PB) is a complex structure located at the junction of the midbrain and hindbrain. Its neurons have diverse genetic profiles and influence a variety of homeostatic functions. While its cytoarchitecture and overall efferent projections are known, we lack comprehensive information on the projection patterns of specific neuronal subtypes in the PB. In this study, we compared the projection patterns of glutamatergic neurons here with a subpopulation expressing the transcription factor *Foxp2* and a further subpopulation expressing the neuropeptide *Pdyn*. To do this, we injected an AAV into the PB region to deliver a Cre-dependent anterograde tracer (synaptophysin-mCherry) in three different strains of Cre-driver mice. We then analyzed 147 neuroanatomical regions for labeled boutons in every brain (n=11). Overall, glutamatergic neurons in the PB region project to a wide variety of sites in the cerebral cortex, basal forebrain, bed nucleus of the stria terminalis, amygdala, diencephalon, and brainstem. *Foxp2* and *Pdyn* subpopulations project heavily to the hypothalamus, but not to the cortex, basal forebrain, or amygdala. Among the few differences between *Foxp2* and *Pdyn* cases was a notable lack of *Pdyn* projections to the ventromedial hypothalamic nucleus. Our results indicate that genetic identity determines connectivity (and therefore, function), providing a framework for mapping all PB output projections based on the genetic identity of its neurons. Using genetic markers to systematically classify PB neurons and their efferent projections will enhance the translation of research findings from experimental animals to humans.

Graphical Abstract (Huang et al.)

[*]Correspondence to: Joel C. Geerling, MD, PhD, joel-geerling@uiowa.edu, PBDB 1320, 169 Newton Rd., Iowa City, IA 52246, 319.353.5425.

Data Availability

The data that support the findings of this study are available from the corresponding author upon reasonable request.

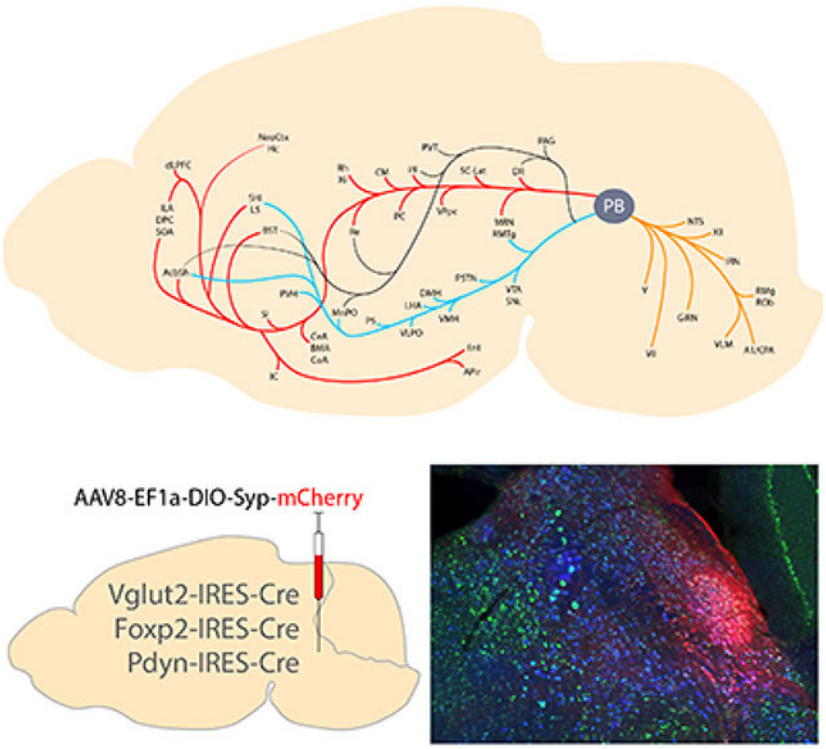

The parabrachial nucleus surrounds the superior cerebellar peduncle at the midbrain-hindbrain junction. Its glutamatergic neurons form subpopulations with distinct genetic identities, two of which express *Foxp2* and *Pdyn*. Here, we detail the location of *Foxp2*- and *Pdyn*-expressing neurons within the larger *Vglut2*-expressing population. We then use Cre-conditional expression of synaptophysin-mCherry to map the efferent projections of each population. Salient findings include the identification of glutamatergic output from the parabrachial nucleus to the rostral entorhinal cortex and lateral superior colliculus, plus an absence of *Foxp2* or *Pdyn* output to the cerebral cortex, basal forebrain, and amygdala.

Keywords

parabrachial complex; entorhinal cortex; amygdalopiriform; superior colliculus; rostromedial tegmental nucleus; dynorphin; Slc17a6; Vglut2

Introduction

The parabrachial nucleus (PB) contains functionally diverse neurons. These neurons receive input from and send output to a broad array of regions throughout the neuroaxis. Different PB subregions receive ascending input from the spinal cord (Bernard et al., 1995; Feil & Herbert, 1995) or the lower brainstem (Herbert et al., 1990; Norgren & Leonard, 1971), as well as descending input from the hypothalamus, amygdala, basal forebrain, bed nucleus of the stria terminalis, and cerebral cortex (Grady et al., 2020; Moga et al., 1990; Tokita et al., 2009). Neurons in and around the PB send output projections to the brainstem and spinal cord (Fulwiler & Saper, 1984; Geerling et al., 2017; Saper & Loewy, 1980; Yoshida et al.,

1997), thalamus (Bester et al., 1999; Krout & Loewy, 2000), hypothalamus (Bester et al., 1997; Fulwiler & Saper, 1984), amygdala (Bernard et al., 1993), bed nucleus of the stria terminalis (Alden et al., 1994), and cerebral cortex (Grady et al., 2020; Saper, 1982).

This groundwork of neuroanatomical knowledge helped identify a role for PB neurons in a wide variety of homeostatic functions. These include taste signaling (Norgren, 1976; Norgren & Leonard, 1971, 1973), hunger (Carter et al., 2015; Carter et al., 2013; Garfield et al., 2015; Kim et al., 2020; Li et al., 2019; Wu et al., 2012), thirst and sodium appetite (Geerling et al., 2011; Lee et al., 2019; Park et al., 2020; Ryan et al., 2017), thermoregulation (Geerling et al., 2016; Nakamura & Morrison, 2008, 2010; Yahiro et al., 2017), nociception (Bester et al., 1995; Chiang et al., 2019), breathing (Chamberlin & Saper, 1994; St John et al., 1972), hypercapnic arousal (Kaur et al., 2013; Kaur et al., 2017), cardiovascular control (Chamberlin & Saper, 1992; Miller et al., 2012), itch (Mu et al., 2017), and alarm (Campos et al., 2018; Palmiter, 2018; Saper, 2016).

In some cases, a specific function has been linked to a subpopulation of PB neurons defined by expression of one or more genes. For example, neurons in the lateral PB that relay skin temperature uniformly express the transcription factor *Foxp2*, and a subset activated by warm temperature expresses the neuropeptide gene *Pdyn* (Geerling et al., 2016). A separate, medial cluster of neurons that express both *Foxp2* and *Pdyn* is implicated in sodium appetite (Gasparini et al., 2019; Geerling et al., 2011; Jarvie & Palmiter, 2017; Lee et al., 2019; Resch et al., 2017). And yet another subset of *Pdyn*-expressing neurons, among or between these populations, has been implicated in mechanosensory feedback signaling for meal termination (Kim et al., 2020).

PB neurons are predominantly glutamatergic, expressing the vesicular glutamate transporter *Slc17a6*/*Vglut2* (Gasparini et al., 2019; Geerling et al., 2017; Miller et al., 2012; Niu et al., 2010; Verstegen et al., 2017a), but we lack a complete map of the efferent projections of glutamatergic neurons in this region. A large subset of glutamatergic PB neurons express the transcription factor *FoxP2* (Geerling et al., 2016; Miller et al., 2012; Verstegen et al., 2017a), and a further subset of these also expresses *Pdyn* (Geerling et al., 2016; Lee et al., 2019; Miller et al., 2012). These genetically distinct subpopulations may have distinct output patterns, but their efferent projections have not been compared or mapped comprehensively. Other investigators targeted subsets of *Vglut2* or *Pdyn* neurons with Cre-conditional vectors in mice (Chiang et al., 2020; Garfield et al., 2014; Kim et al., 2020; Lee et al., 2019) without showing or systematically analyzing their axonal projections, and the only information available regarding the efferent projections of *Foxp2* neurons in the PB derives from retrograde labeling in rats (Shin et al., 2011).

Having cell-type-specific information about the overall projection patterns of these PB subpopulations would improve our ability to predict and test their functions. Here we use Cre-conditional labeling in mice to map and compare the whole-brain efferent projections of *Vglut2*-, *Foxp2*- and *Pdyn*-expressing neurons in the PB region.

Materials and Methods

Mice.

All mice were group-housed in a temperature- and humidity-controlled room on a 12/12-hour light/dark cycle and with *ad libitum* access to water and standard rodent chow. Overall, we used n=18 mice, both male (n=13) and female (n=5), ranging in age from 8 to 31 weeks (19–35 g body weight). We used a variety of knockin Cre and Cre-reporter mice; detailed information about each strain is in Table 1. All Cre-driver and Cre-reporter mice were hemizygous and maintained on a C57BL6/J background. We also used tracing data from several of these mice in a separate study that focused exclusively on interconnectivity between the cerebral cortex and PB (Grady et al., 2020). All experiments were conducted in accordance with the guidelines of the Institutional Animal Care and Use Committee at the University of Iowa.

Stereotaxic injections.

Mice were anesthetized with isoflurane (0.5–2.0%) and placed in a stereotactic frame (Kopf 1900 or 940). We made a midline incision and retracted the skin to expose the skull and identify bregma, then drilled a small burr hole above the right PB region. Through a pulled glass micropipette (20–30 μm inner tip diameter), we injected AAV8-hEf1a-DIO-synaptophysin-mCherry (AAV8-DIO-Syp-mCherry, 2.5×10^{13} pfu/mL; purchased from Dr. Rachel Neve at the Massachusetts Institute of Technology McGovern Institute for Brain Research Viral Vector Core). Injection volumes ranged 20–100 nL (80–100 nL in *Vglut2-IRES-Cre*, 60–80 nL in *FoxP2-IRES-Cre*, and 20 nL in *Pdyn-IRES-Cre* mice). We used slightly larger injection volumes in Vglut2 cases to cover a larger extent of the PB per case and smaller injection volumes in Pdyn cases because pilot injections with larger volumes than this resulted in substantial transduction of neurons outside the PB. In each case, we targeted the parabrachial nucleus with coordinates 4.77–5.25 mm caudal to bregma, 0.92–1.40 mm right of midline, and 3.55–3.85 mm deep to bregma. Each injection was made over a 5-minute period, using picoliter air puffs through a solenoid valve (Clippard EV 24V DC) pulsed by a Grass stimulator. The pipette was left in place for an additional 3–5 minutes, then withdrawn slowly before closing the skin with Vetbond (3M). Meloxicam (1 mg/1 kg) was provided for postoperative analgesia. AAV-injected mice were allowed to survive for 3–5 weeks after surgery to allow optimal production of Cre-conditional proteins and traffic into synaptic boutons (Vglut2 cases 26–35 days; FoxP2 cases 20–35 days; Pdyn cases 32 days).

Perfusion and tissue sections.

Mice were anesthetized with a mixture of ketamine-xylazine (i.p. 150 and 15 mg/kg, respectively, dissolved in sterile 0.9% saline), then perfused transcardially with phosphate-buffered saline (PBS), followed by 10% formalin-PBS (SF100–20, Fischer Scientific). After perfusion, the brain was removed and fixed overnight in 10% formalin-PBS. We sectioned the brains into 40 μm-thick coronal slices using a freezing microtome and collected tissue sections into separate, 1-in-3 series. Sections were stored in cryoprotectant solution at −20 °C until further processing.

Immunohistology.

For immunofluorescence labeling, we removed the tissue sections from cryoprotectant and rinsed them in PBS before loading them into a primary antibody solution. Primary antisera (see Table 2 for details) were added to a PBS solution of 0.25% Triton X-100 (BP151–500, Fisher), 2% normal donkey serum (NDS, 017-000-121, Jackson ImmunoResearch), and 0.05% sodium azide (14314, Alfa Aesar) as a preservative (PBT-NDS-azide). We incubated these sections overnight at room temperature on a tissue shaker. The following morning, the sections were washed 3× in PBS and incubated for 2 hours at room temperature in PBT-NDS-azide solution containing species-specific donkey secondary antibodies. These secondary antibodies were conjugated to Cy3, Cy5, Alexa Fluor 488, or biotin (Jackson ImmunoResearch; each diluted 1:500–1,000). When a biotinylated secondary antibody was used, we incubated tissue sections for an additional 2 hours in streptavidin-Cy5 (#SA1011; Invitrogen) prepared in PBT-NDS-azide. These sections were then washed 3× in PBS, mounted on glass slides (#2575-plus; Brain Research Laboratories), and coverslipped using Vectashield with DAPI (Vector Labs). Slides were stored in slide folders at 4 °C until imaging.

For brightfield labeling (immunohistochemistry), we removed tissue sections from cryoprotectant, rinsed them in PBS, then incubated them in hydrogen peroxide (0.3% in PBT-Az; #H325–100, Fisher) for 30 minutes to quench endogenous peroxidase activity. After 3× washes in PBS, we loaded sections into PBT-NDS-azide containing rabbit anti-dsRed and incubated them overnight, at room temperature, on a tissue shaker. After 3 PBS washes the following morning, we incubated sections for 2 hours in a 1:500 solution of biotinylated donkey anti-rabbit (#711-065-152; Jackson) in PBT-NDS-azide. Sections were washed 3× and placed for 1 hour in avidin-biotin complex (Vectastain ABC kit PK-6100; Vector), washed 3× in PBS, and incubated in nickel-diaminobenzidine (NiDAB) solution for 10 minutes. Our stock DAB solution was prepared by adding 100 tablets (#D-4418, Sigma, Saint Louis, MO) into 200 mL ddH_2O, and then filtering it. We then used 1 mL of this DAB stock solution, with 300 μL of 8% nickel chloride (#N54–500, Fisher Chemical) per 6.5 mL PBS. After 10 minutes in NiDAB, we added hydrogen peroxide (0.8 μL of 30% H_2O_2 per 1 mL PBS-DAB) and swirled sections for 2–5 minutes until observing black (nickel-DAB) color change. After two rapid PBS washes, we wet-mounted one or more sections and checked them in a light microscope to ensure optimal staining. Finally, after washing sections an additional 3× in PBS, we ordered and mounted them on glass slides. Slides were air-dried then dehydrated in an ascending series of alcohols and xylenes, then coverslipped with Cytoseal 60 (#8310–16 Thermo Scientific).

Nissl counterstaining.

After whole-slide imaging (described below), all slides were Nissl-counterstained then re-imaged. The coverslips were removed by soaking in xylenes for up to a week. After rehydration through 1-minute dips in a graded series of alcohols, we rinsed the slides in water and dipped them in a 0.125% thionin solution (Fisher Scientific) for 1 minute. Slides were rinsed in water until the solution cleared, then dehydrated in a series of ethanol solutions. The slides were placed in 50% EtOH, 70% EtOH, 400mL of 95% EtOH with 10

drops of glacial acetic acid, 95% EtOH, 100%, and 100% EtOH, and two xylene solutions. Afterwards, the slides were coverslipped with Cytoseal.

Fluorescence *in situ* hybridization.

To label neurons that express mRNA for *Slc17a6*/*Vglut2* in n=2 AAV-injected cases (1280 and 1281) and in n=3 male Cre-reporter mice for *Vglut2*, or *Pdyn* in n=3 AAV-injected cases (1812, 1813, and 1814), we used RNAscope Fluorescent Multiplex Detection Reagents (ref# 320851; Advanced Cell Diagnostics). For background cytoarchitecture in the AAV-injected Vglut2 cases, we also labeled ubiquitin (*Ubc*) mRNA.

The afternoon before hybridization, we removed six tissue sections through the PB region from cryoprotectant, rinsed them in PBS at room temperature, and then mounted them on glass slides to dry overnight at 4 °C. In the morning, we outlined sections using a Super-HI PAP pen (Research Products Incorporated) and vacuum grease (Dow Corning) to form a hydrophobic barrier, then washed sections in PBS for 2 minutes, twice, at room temperature. We then covered sections with Protease IV in glass petri dishes floating in a 40 °C water bath for 30 minutes. After PBS 2 × 2 minute washes, we incubated sections in a combination of two probes (Mm-Slc17a6-C3, #319171-C3 and Mm-Ubc #310771 or Mm-Pdyn-C3 #318771-C3; ACD) for 2 hours at 40 °C. After that, we added amplification reagents 1–4 in series, for 15–30 minutes each, at 40 °C, with 2 × 2 minutes in RNAscope wash buffer (#320058; diluted 1:50 in ddH20) between each step.

After finishing the RNAscope protocol, we used immunofluorescence to label mCherry. Sections were incubated in PBT-azide solution with primary antibody (rat anti-mCherry, see Table 2) overnight at 4 °C, then washed with PBS the next morning and incubated in Cy3-donkey anti-rat (1:1000 in PBT-azide; #712-165-153, Jackson ImmunoResearch) for 2 hours at room temperature. After a final PBS wash, we coverslipped slides using Vectashield with DAPI.

Imaging, figures, and analysis.

All slides were scanned using an Olympus VS120 microscope. For brightfield images of NiDAB and then Nissl-counterstained sections, we used a ×20 (NA 0.75) or ×40 (NA0.95) objective with extended focal imaging (EFI) to collect and combine in-focus images from 11 focal planes through the tissue. After reviewing whole-slide images in OlyVIA or VS-ASW software (Olympus), we collected additional EFI or multifocal image stacks at higher magnifications in some regions of interest. To collect images from the lateral PB of neurons containing *Slc17a6*/*Vglut2* mRNA and L10GFP Cre-reporter for Vglut2, we used the ×25 water immersion objective on a laser-scanning confocal microscope (TCS SP5II, Leica).

To collect epifluorescence images of immunofluorescence and RNAscope-labeled sections through the injection site or lateral hypothalamus in a subset of cases, we began by using an ×10 (NA 0.40) objective to scan the full slide, then collected ×20 EFI images encompassing each region of interest. Finally, in regions containing Syp-mCherry-expressing neurons, we collected ×40 Z-stacks encompassing all these neurons at each level of the injection site, for co-localization cell counts. For each slide, this produced a Virtual Slide Image (VSI) file

containing a single, ×10, whole-slide layer, plus separate layers with ×20 EFI and in some cases, ×40 Z-stacks, in regions of interest for analysis or figures.

We opened each VSI file in Cellsens (Olympus), then scanned through every Z-plane in each ×40 image stack (containing every rostro-caudal level through the injection site) and marked every neuron with Cy3 immunofluorescence labeling for (Syp-)mCherry. We used a conservative set of criteria to count neurons, only counting cells with a definite nuclear void that was present and fully in-focus in at least 1 focal plane in the Z-stack. After marking all Syp-mCherry-expressing neurons, we returned to each cell and examined every focal plane containing its nucleus and cytoplasm for punctate *Slc17a6*/Vglut2 mRNA labeling (*Vglut2-IRES-Cre* cases 1280 and 1281) or *Pdyn* mRNA labeling (*Pdyn-IRES-Cre* cases 1812, 1813, and 1814), using a conservative criterion of at least 10 mRNA dots present and in-focus in the area bounded by Syp-mCherry labeling in that neuron. In tissue with immunofluorescence labeling for FoxP2 and (Syp-)mCherry, we assessed each Syp-mCherry-expressing neuron for nuclear FoxP2-immunoreactivity (*Foxp2-IRES-Cre* cases 1404 and 1405 and *Pdyn-IRES-Cre* cases 1812 and 1814). For each of these combinations, we divided the number of double-labeled neurons by the total number of Syp-mCherry labeled neurons across all sections in each case to calculate the percentage of neurons expressing the mRNA or protein in question. We did not use an Abercrombie correction factor because the result of interest was the percentage of Syp-mCherry-transduced neurons that contain a particular mRNA or protein, which stems from a binary rating for each neuron; applying a counting correction would not change this result, and estimating the total number of neurons transduced is not a relevant endpoint in this study. We did not count the overall numbers of FoxP2-immunoreactive nuclei, *Slc17a6*/*Vglut2* mRNA-, or *Pdyn* mRNA-expressing cells because these numbers were not of interest in this study, where the proportion of overall cells that were transduced to express Syp-mCherry in each population was very small.

To compare the overall spatial distribution of transduced neurons in each injection site, we plotted the core cluster of Syp-mCherry-expressing neurons in each case onto three template levels of the PB (approximate bregma levels −5.0, −5.2, −5.4) atop landmarks derived from Nissl-counterstained images of the PB region. We overlaid these injection site outlines in Adobe Illustrator and applied color and transparency (50% opacity) to produce the comparisons in Figure 4. Nissl-counterstained sections through the full injection site from each case (including sections rostral or caudal to the PB in some cases) are shown in the Supplemental Figure.

In all cases, we immunolabeled, imaged, and analyzed every section from at least one 1-in-3 series of sections through the full brain, from the olfactory bulbs to the cervical spinal cord. Throughout this paper, we will use the term “boutons” to refer to punctate, NiDAB labeling of Syp-mCherry. Immunoelectron and light microscopy studies uniformly localize synaptophysin to presynaptic boutons, where it is an integral membrane protein in all synaptic vesicles (Calhoun et al., 1996; Wiedenmann & Franke, 1985). We identified Syp-mCherry-labeled boutons in NiDAB-labeled images (without Nissl counterstaining), then compared the locations of labeled boutons in these images side-by-side with subsequent images of the same sections after Nissl counterstaining to more precisely identify

neuroanatomical loci based on the local cytoarchitecture. We scored the density of Syp-mCherry-labeled boutons in each brain region on a semi-quantitative (0–4) scale. For brain regions with scattered, minimal labeling, we assigned the intermediate designation of “trace” labeling. Our reference standards are shown in Figure 6. Two independent raters (DH & JCG) scored every region from each brain and reviewed all results together, using the same reference standards to reach consensus. We compiled this full-brain information for every PB-injected case from every genotype to produce the comparisons in Figure 6.

We also developed a neural network-based Python script to plot Syp-mCherry-labeled boutons for illustrations. This script combines two separate algorithms, in series, to label boutons with a high degree of confidence; a “proposal” intensity-based algorithm, followed by a “confirmation” convolutional neural-network based algorithm. A full-resolution TIFF (346 nanometers per pixel) was exported from VS-ASW (Olympus) and imported into Python. The proposal algorithm passes the image through a Gaussian filter to smooth out small histological artifacts, then searches for groups of pixels that are darker by 3 grayscale values than the surrounding tissue (15 surrounding pixels). These pixels are considered potential boutons to be analyzed by the confirmation algorithm.

The confirmation algorithm is a convolutional neural network that inputs a 15-by-15 pixel subsample of the larger image, centered on the potential bouton. As positive training data, this algorithm uses 173,934 boutons that were labelled manually from 17 tissue sections from two brains. As negative training data, we randomly selected 5,000 portions of these images, discarding any that overlapped by more than 50% any of the 15-by-15 (225-pixel) frames surrounding manually-labelled boutons. These training data were fed into a neural network with several convolutional, max-pooling, and fully connected layers, which outputted a probability of the potential bouton being labeled as a true bouton by a human annotator. The full algorithm is available at https://github.com/GeerlingLab/Parabrachial_efferents. We used this algorithm to identify and plot boutons in matched subsets of 27 sections selected from one representative brain chosen from each genotype (1280 *Vglut2*, 1405 *Foxp2*, 1812 *Pdyn*). Each bouton location was output as a circle (radius 5 pixels) filled with red (*Vglut2*), blue (*Foxp2*), or green (*Pdyn*). These images had the same dimensions and pixel resolution as the input image, with the background color set as transparent, and were exported and compressed to PNG. Next, in Adobe Illustrator, we aligned each PNG file containing color boutons in a separate layer atop the source (TIFF) histological image from each brain section. In another layer, we aligned a Nissl-counterstained image of the same section. We used the aligned Nissl cytoarchitecture in this image to trace the brain borders, major white matter tracts, and cerebral ventricles for illustrations. We also used Nissl cytoarchitecture in the counterstained section to confirm the neuroanatomical location of Syp-mCherry-labeled boutons in the NiDAB (pre-counterstaining) source image and in the plotted PNG overlay.

We Z-projected confocal stacks and merged color channels using FIJI (ImageJ). For other figures that contain brightfield or fluorescence images, we used Adobe Photoshop to crop bitmap images from VS-ASW or OlyVIA (Olympus), adjust brightness and contrast, or combine raw fluorescence data for multicolor combinations. We added lettering and made all drawings in Adobe Illustrator. Scale bars were traced atop calibrated lines in OlyVIA to

produce a clean white or black line. To compare the diameters of Syp-mCherry-immunolabeled boutons in the thalamus of case 1280, we opened whole-slide images in cellSens (Olympus) and measured the long-axis diameter of 30 punctae, chosen at random from the lateral aspect of the parvicellular ventral posterior thalamic nucleus or from the overlying parafascicular thalamic nucleus. We then used Prism 8 (GraphPad) to produce a histogram (0.5 μm bins) comparing the distribution of bouton sizes from each region.

Nomenclature.

Nomenclature in this paper derives from original neuroanatomical work in the peer-reviewed literature. For the PB, this literature stems from the cytoarchitecture-based taxonomy proposed in rats by Fulwiler and Saper (1984), but also includes subsequent work clarifying subnuclear anatomy in mice (Geerling et al., 2016; Geerling et al., 2017; Kaur et al., 2013; Verstegen et al., 2017b). For other brain regions, we used nomenclature that has been adopted by at least one of the two widely used mouse brain atlases (Dong, 2008; Paxinos & Franklin, 2013).

Results

Distributions of *Vglut2*-, *Foxp2*-, and *Pdyn*-expressing PB neurons.

We began by examining the distribution of PB neurons that express *Vglut2* and the transcription factor FoxP2. To do this, we immunolabeled the FoxP2 protein in Cre-reporter mice where GFP expression identifies neurons with current or previous *Vglut2* expression (*Vglut2-IRES-Cre*;*R26-lsl-L10GFP*). Consistent with evidence that most PB neurons are glutamatergic (Geerling et al., 2017; Niu et al., 2010), GFP-expressing neurons filled the PB. Here and in most surrounding regions, GFP-expressing neurons uniformly contained *Slc17a6*/*Vglut2* mRNA (Figure 1), with the prominent exception of neurons in the locus coeruleus (LC), which also expressed GFP, which are known to lack *Vglut2* expression in adults (Stornetta et al., 2002). All subregions of the PB contained GFP-expressing neurons, and a subset of these contained nuclear immunoreactivity for FoxP2 (Figure 1). Conversely, all PB neurons with nuclear FoxP2 immunoreactivity also contained GFP, except for a cluster of FoxP2+ neurons at the caudal, ventrolateral edge of the PB, which form the previously described, GABAergic population we named the “caudal Kolliker-Fuse (KF)” (not shown here; see Geerling et al., 2017). Besides this small population, FoxP2+ neurons form a dense cluster in the lateral subdivision of the PB, spanning its superior lateral (PBsL), rostral-to-external-lateral (PBreL), central lateral (PBcL), and dorsal lateral (PBdL) subnuclei. Fewer FoxP2+ neurons scatter medially, except for a dense, caudal cluster in the pre-locus coeruleus (pre-LC, Figure 2g).

Next, we immunolabeled FoxP2 in GFP reporter mice for *Pdyn* (*Pdyn-IRES-Cre*;*R26-lsl-L10GFP*), which allowed us to identify neurons with current or previous expression of *Pdyn*. Amid the same overall distribution of FoxP2-immunoreactive nuclei, a large subset co-localized with GFP, indicating current or previous expression of *Pdyn* (Figure 2). Many other FoxP2-immunoreactive neurons lacked GFP, but a large majority of GFP+ neurons in the PB contained nuclear FoxP2 immunoreactivity, indicating that most *Pdyn* neurons in this region represent a subpopulation of PB FoxP2+ neurons. These neurons formed a primary

cluster in PBdL (Figure 2e) extending rostrally through PBcL, but tapering into fewer, scattered neurons among the dense FoxP2+ population in PBreL (Figure 2b). Medial and caudal to PBdL, these neurons extended across the superior cerebellar peduncle and mesencephalic trigeminal nucleus to form a caudal cluster in the pre-LC (Figure 2h).

Injection Sites.

We injected a vector that delivers a Cre-conditional synaptic marker, synaptophysin-mCherry (AAV8-hEf1a-DIO-synaptophysin(Syp)-mCherry), into the PB of *Vglut2-IRES-Cre*, *Foxp2-IRES-Cre*, and *Pdyn-IRES-Cre* mice. In *Vglut2-IRES-Cre* cases, Syp-mCherry expression was restricted to neurons with mRNA for *Vglut2* (1,184 of 1,186 counted across n=2 cases, Table 3; Figure 3a–f). Injections of the same vector into the PB of *FoxP2-IRES-Cre* mice transduced fewer neurons, with Syp-mCherry expression restricted to neurons with nuclear immunoreactivity for FoxP2 (324 of 329 counted across n=2 cases, Table 3; Figure 3g–l). Injections into *Pdyn-IRES-Cre* mice produced Syp-mCherry expression in neurons that contain *Pdyn* mRNA (233 of 235 neurons counted across n=3 cases, Table 3; Figure 3m–o), and most contained nuclear immunoreactivity for FoxP2 (159 of 178 counted from n=2 cases, Table 3; Figure 3p–u).

Overall, we analyzed 11 cases with injection sites in or largely overlapping the PB. Figure 4 shows the location and extent of the core cluster of neurons expressing Syp-mCherry in the PB at three, rostral-to-caudal levels in each case. The full, rostrocaudal extent of Syp-mCherry immunoreactivity in each injection site is shown in the Supplemental Figure.

As expected from the broad distribution of *Vglut2*-expressing neurons in and around the PB, *Vglut2-IRES-Cre* cases had the most neurons expressing the Cre-conditional construct. Each individual injection transduced neurons across several PB subnuclei and, in combination, these four cases covered the entire PB. Most injection sites included at least a few Syp-mCherry-expressing neurons dorsal to the PB, in the cuneiform nucleus and inferior colliculus. So while our combined cases represent the full set of efferent projections from the PB, a small subset of projections arise from neurons neighboring the PB. Indeed, as shown below, some cases had Syp-mCherry-labeled boutons in the ventromedial medulla (the primary efferent target of glutamatergic neurons in the cuneiform nucleus; Caggiano et al., 2018) or in the medial geniculate nucleus of the thalamus (MGN, the primary efferent target of neurons in the inferior colliculus; Kudo & Niimi, 1978).

Injections of the same vector in *Foxp2-IRES-Cre* mice transduced a more restricted subset of PB neurons, similar to the distribution of FoxP2 immunoreactive neurons shown in Figures 1–2. Injections in *Pdyn-IRES-Cre* mice transduced an even more restricted subpopulation with a pattern similar to the GFP reporter for *Pdyn* in Figure 2.

Distributions of Syp-mCherry-labeled boutons.

The brain-wide distribution of anterogradely labeled boutons in an exemplary case from each genotype is shown in Figure 5. We present the rostralto-caudal distribution of brain regions that receive input from the PB region, complementing this information with photomicrographs from additional cases to highlight salient differences in projection

patterns between genotypes or among injection site locations. Going forward, we will use the terms “Vglut2,” “Foxp2,” and “Pdyn” rather than the full genotype.

Overall, Vglut2 cases had much more extensive labeling across a greater number of brain regions, extending from the frontal pole back through the spinomedullary junction. FoxP2 and Pdyn cases had labeling in subsets of these regions, primarily in the diencephalon, but FoxP2 and Pdyn projections avoided the cerebral cortex, basal forebrain, amygdala, and several other regions with heavy labeling in Vglut2 cases. Ipsilateral was stronger than contralateral labeling in all regions, with two notable exceptions, the ventral tegmental area (VTA) and the lateral aspect of the parvicellular ventroposterior thalamic nucleus (VPpc), as described below.

Cerebral cortex.

We found extensive projections to the cerebral cortex in all Vglut2 cases (see also Grady et al., 2020). These projections were most extensive in cases with injections covering the medial PB (cases 0147, 1280) and less dense after injections that were centered laterally (1281) or rostrally and dorsally (0017). Throughout the prefrontal cortex, moderately dense Syp-mCherry labeling pervaded the deep layers, from the genu of the corpus callosum up to the frontal pole (Figure 5a1–c1). At the caudal end of this prefrontal expanse, immediately rostral to the corpus callosum, a dense collection of boutons appeared in the medial prefrontal cortex, within the ventral infralimbic area and dorsal peduncular cortex (Figure 5b1). In the infralimbic area, Syp-mCherry labeled boutons concentrated in layer 5, some forming linear groupings that had the appearance of coating the apical dendrites of pyramidal neurons extending medially from layer 5 (Figure 15a). Immediately ventral to this, a dense collection of boutons filled the molecular layer (layer 1) of the dorsal peduncular cortex (Figure 7a). Many labeled axons and boutons also extended ventrally, into a rostral-ventral region previously referred to as the “septo-olfactory” area (Saper, 1982; Saper & Loewy, 1980) (Figure 5a1–c1; Figure 7b) or caudally, into the septum pellucidum (below).

Overall, the mid-insular cortex contained the densest collection of Syp-mCherry-labeled boutons in the cerebral cortex (see also Grady et al., 2020). This terminal field was prominent at all brain levels within 1mm of (rostral or caudal to) the midline decussation of the anterior commissure (Figure 5e1–h1). After injections centered in the medial PB (cases 0147, 1280), Syp-mCherry-labeled boutons within the insular cortex covered nearly all layers in the “dysgranular” and granular areas here, with additional boutons extending medially to reach a zone immediately dorsal to the principal claustrum (Figure 7d). In contrast, an injection centered in the external lateral PB subnucleus (1281) produced a much more restricted distribution of boutons in the insular cortex, concentrating over layers 2–3, with few boutons in deep cortical layers (Figure 7e).

Further rostrally, labeling within the insular cortex became less dense and split into a dorsal band above, and a thin ventral band below the large agranular subdivision, which never contained more than trace labeling (Figure 5b1–d1). The dorsal band of boutons, above the agranular insular area, appeared to supply the aforementioned terminal field throughout the deep layers of the dorsolateral prefrontal cortex. In contrast, the thinner, ventral band of

fibers and boutons extended ventrally and rostrally, coursing through the endopiriform nucleus, and turned medially then dorsally into the septo-olfactory area and medial prefrontal cortex (Figure 5b1–d1).

At more caudal levels, Syp-mCherry-labeled boutons continued from the heavy mid-insular terminal field into a narrow band through the caudal, “visceral” area of the insular cortex (Figure 5h1–k1). From there, labeling became much lighter through the perirhinal cortex, then aggregated into a dense collection of boutons in layer 5 of the rostral entorhinal cortex (Figure 5n1–o1; Figure 7c). Nearby, another dense, prominent cluster of boutons filled the amygdalopiriform transition area (APir), a transitional cortex bordering the posterior amygdala, piriform cortex, and entorhinal cortex (Figure 5n1–o1; Figure 7c).

Outside the areas described above, no other regions of the cerebral cortex had dense collections of boutons. However, cases with injection sites centered in the medial PB (0147, 1280) had scattered, rare Syp-mCherry-labeled boutons (trace labeling) in every cortical area, including the hippocampus.

In sharp contrast to Vglut2 cases, Pdyn and Foxp2 cases had virtually no cortical labeling. Two Pdyn injections transduced a small number of neurons in the locus coeruleus neurons (1 and 3 neurons contained both Syp-mCherry and tyrosine hydroxylase immunofluorescence in cases 1814 and 1812, respectively; not shown). Both cases had scattered, trace labeling without aggregations of boutons in any areas of the cerebral cortex. Other than this, cortical labeling was non-existent in FoxP2 and Pdyn cases.

Septum and basal forebrain.

The septum pellucidum contained a complex set of terminal fields in continuity with labeling in the septo-olfactory area and medial prefrontal cortex. All Vglut2 cases contained dense concentrations of boutons in two subregions: the rostral or intermediate part of the lateral septum (Figure 5c1) and the septohippocampal nucleus (Figure 5d1). In each, dense aggregates of Syp-mCherry-labeled boutons formed clusters that appeared to outline the soma and proximal dendrites of individual neurons (Figure 15b). In contrast to Vglut2 cases, FoxP2 cases contained light labeling in the intermediate or rostral part of the lateral septum, and Pdyn cases contained only trace labeling here. The medial septum contained no more than light or trace labeling, with no dense collections of boutons in any case.

In Vglut2 cases, several basal forebrain nuclei received extensive input. In contrast, FoxP2 cases contained very little labeling, and Pdyn cases contained virtually none in the basal forebrain. All Vglut2 cases had dense labeling throughout the substantia innominata, which extends from the lateral preoptic area to the amygdala (Figure 5e1–j1; Figure 8a). Ventrally and rostrally contiguous regions of the diagonal band and magnocellular nuclei contained slightly less labeling, as did a rostral zone between the diagonal band, medial septum, and shell of the nucleus accumbens designated by some as the rostral extent of the lateral preoptic area (Dong, 2008). Caudally, the region with corticopetal basal forebrain neurons that are homologous to the primate basal nucleus of Meynert and distribute dorsally into the ventral globus pallidus and internal capsule (Chen et al., 2015; Guo et al., 2016; Price & Stern, 1983; Saunders et al., 2015) contained moderately dense labeling. In every Vglut2

case, this labeling extended dorsally as a linear streak of Syp-mCherry-labeled boutons, running between the striatum and external globus pallidus at all levels containing these basal ganglia structures (Figure 5h1–j1; Figure 8a).

Basal ganglia.

In addition to labeling extending dorsally from the substantia innominata into the ventral globus pallidus, all Vglut2 cases contained light labeling throughout the ventral caudate-putamen and nucleus accumbens (Figure 8a). The injection site centered in the external lateral PB (1281) produced the fewest, while injections into the center (0147, 1280) or rostral-dorsal (0017) aspects of the PB produced more extensive labeling in the striatum.

FoxP2 and Pdyn cases did not have any labeled boutons in the striatum, except in the caudal shell of the nucleus accumbens, immediately rostral to the bed nucleus of the stria terminalis (BST; Figure 5e2–f2). This region of the nucleus accumbens contained light labeling across genotypes, with slightly more labeling in Vglut2 cases.

In all Vglut2 cases, the ventral two-thirds of the external globus pallidus contained light labeling, mirroring the adjacent striatum (Figure 8a). This light, scattered input had a dorsal-to-ventral gradient of increasing density, and (as in the striatum) case 1281 had less labeling than the other three. Foxp2 and Pdyn cases had no labeling in the globus pallidus.

The internal globus pallidus, also known in rodents as the entopeduncular nucleus, contained a moderate density of Syp-mCherry-labeled boutons in every Vglut2 case, but no labeling in any Foxp2 or Pdyn cases.

The subthalamic nucleus (STN) contained a variable degree of labeling in different Vglut2 cases. Consistent with evidence that the pedunculopontine tegmental area (immediately rostral and medial to the PB) provides input to this nucleus (Canteras et al., 1990; Jackson & Crossman, 1983), the most rostral and medial injection (case 0017) produced heavy labeling in the STN, while the most lateral injection (case 1281) produced the least (Figure 8b–c) and the remaining two cases had intermediate densities. No Foxp2 or Pdyn cases had any labeling in the STN, despite labeling in all cases in an adjacent structure in the hypothalamus, the parasubthalamic nucleus (PSTN, see below).

Amygdala.

The amygdala contained among the densest labeling in Vglut2 cases. In contrast, FoxP2 and Pdyn cases had virtually no labeling in the amygdala.

In all Vglut2 cases, a dense field of Syp-mCherry-labeled boutons continued laterally and caudally from the basal forebrain to form a dense terminal field in the anterior amygdalar area and the central nucleus of the amygdala (CeA). This dense terminal field extended ventrally, through the BMA and into the cortical amygdalar area (CoA), excluding its molecular layer (Figure 5j1–l1; Figure 9a). Where the Vglut2 terminal field in the CeA-BMA-CoA continuum merged rostrally into the anterior amygdalar area, it sharply outlined the underlying nucleus of the lateral olfactory tract, which was devoid of labeling in all cases (Figure 5h1–j1). No FoxP2 or Pdyn cases had more than sparse, fragmentary labeling in the

amygdala, and most sections through this region had no labeling at all (Figure 5j2–l3; Figure 9b).

In Vglut2 cases, the medial nucleus of the amygdala (MeA) also contained moderately dense labeling. We also found dense labeling in a small, rostral portion of the lateral amygdalar nucleus. The basolateral and intercalated nuclei contained light labeling overall. Ventrolateral to the posterior BLA, at the caudal-lateral border between the amygdala and piriform cortex, we also found a dense cluster of labeled boutons in the APir, as described above (Figure 5m1–o1; Figure 7c).

Consistent with anterograde tracing results in rats (Bernard et al., 1993), injection sites into different subregions of the mouse PB produced strikingly different patterns of labeling in the amygdala. For example, case 1281 had incredibly dense labeling in the lateral and lateral capsular subdivisions (Figure 9d), while 1280 had evenly dense labeling across all CeA subdivisions, 0147 had denser labeling in the medial CeA than in its lateral and lateral capsular subdivisions (Figure 9c), and 0017 had labeling almost exclusively in the medial subdivision. Compared to other cases, 1281 also had denser labeling in the MeA, but lighter labeling in the BMA and cortical amygdala.

Bed nucleus of the stria terminalis.

The BST, which sits on the opposite side of the basal forebrain from the amygdala, received similarly complex input (Figure 5f1–g3; Figure 9e–f). Like the amygdala, Vglut2 cases had substantially more labeling here, but in contrast to the amygdala, all FoxP2 and Pdyn cases had light labeling in the BST.

Among Vglut2 cases, 1281 had the densest and most restricted pattern, with dense Syp-mCherry-labeled boutons filling the oval BST subnucleus (dorsal to the anterior commissure) and moderately dense boutons in the fusiform subnucleus (ventral to the anterior commissure; Figure 9e). Case 1280 had a more evenly dense pattern of labeling across the anterior BST, and 0147 had an intermediate density in a similar pattern. Case 0017 had light labeling in the BST overall, with only trace labeling in the oval subnucleus. In all cases, labeling was denser in the anterior BST and tapered caudally. Dorsal and caudal to the BST, the stria terminalis itself contained punctate labeling (putatively in boutons) along its arc between the BST and the CeA, most prominently in cases 1281 and 1280.

FoxP2 and Pdyn cases had significantly less labeling in the BST (Figure 9f), with no prominent labeling in any subnucleus. The oval BST subnucleus never contained more than trace labeling in these cases, while the fusiform, anterolateral, and anteromedial subnuclei contained light labeling in all cases.

Lamina terminalis.

Projections to the subfornical organ were light, but similar in all cases. Vglut2 case 1281 and two Pdyn cases had denser labeling, indicating that this light projection originates from the lateral PB. In contrast, the organum vasculosum of the lamina terminalis, which surrounds the anterior (optic recess of the) third ventricle, contained minimal to no labeling, though it

was difficult to determine the exact boundary of this nucleus amid the massively dense PB projection to surrounding regions of the preoptic area in every cases.

Preoptic area and hypothalamus.

Among all brain regions, the preoptic area and hypothalamus contained the most similar pattern and density of labeling in Foxp2 and Pdyn cases, relative to Vglut2 cases, with a few notable exceptions.

In all cases, Syp-mCherry boutons filled a contiguous zone through the ventromedial preoptic area (VMPO, Figure 5e1–f3), median preoptic nucleus (MnPO, Figure 5f1–3) and ventrolateral preoptic area (VLPO, Figure 5g1–3). Labeled boutons extended dorsally from the VLPO and through the medial preoptic area to form a moderately dense terminal field in the parastrial nucleus just medial to the ventral BST (Figure 5g1–g3; Figure 9f). In contrast, the medial preoptic area contained light labeling, with minimal to no labeling in the medial preoptic nucleus. The lateral preoptic area had moderately dense labeling in all Vglut2 cases, as detailed above, but virtually none in FoxP2 and Pdyn cases.

Several hypothalamic areas contained similar labeling across genotypes (see Figure 7). The anterior nucleus never had more than light labeling, while the suprachiasmatic nucleus contained little to no labeling. In contrast, the retrochiasmatic area, paraventricular hypothalamic nucleus (PVH), arcuate nucleus (Arc), dorsomedial hypothalamic nucleus (DMH), lateral hypothalamic area (LHA), and PSTN contained similarly prominent labeling in all genotypes, with denser labeling in Vglut2 cases (Figure 5h1–n3). In the LHA, the dense concentration of Syp-mCherry-labeled boutons (Figure 5k1–3) closely tracked the distribution of neurons immunoreactive for the neuropeptide hypocretin/orexin. The striking correspondence was most evident in Pdyn cases (Figure 10).

The most conspicuous differences between cases involved the ventromedial nucleus of the hypothalamus (VMH, Figure 11). Vglut2 cases with injections centered in the medial PB (0147, 1280) had a light or moderate labeling density in the VMH, while an injection site in the lateral PB (1281) produced in the VMH the densest Syp-mCherry-labeled terminal field in any of our cases (Figure 11a). FoxP2 cases with injections that extended rostrally in the lateral PB (1405, including the rostral-to-external lateral and central lateral subnuclei) produced an intermediate density of labeling in the VMH (Figure 11b). In sharp contrast, the VMH was virtually empty in Pdyn cases, despite dense Syp-mCherry labeling in the overlying DMH and LHA (Figure 11c). This absence of labeling was the most prominent difference between Pdyn and FoxP2 cases.

Thalamus.

The paraventricular thalamic nucleus (PVT) contained a moderate density of Syp-mCherry labeling in all cases, along its full rostro-caudal extent, with slightly denser labeling in Vglut2 cases (Figure 5h1–l3). At mid-ventral levels of the thalamus, the reuniens (Re), rhomboid (Rh), and xiphoid (Xi) nuclei contained moderately dense labeling in all Vglut2 cases and lighter labeling in FoxP2 and Pdyn cases (Figure 5j1–k3; Figure 12a–b). In the epithalamus, the lateral habenular nucleus received light labeling in all Vglut2 and most FoxP2 cases, but none in Pdyn cases. The centromedian (CM) and parafascicular (PF)

thalamic nuclei contained variably dense labeling across Vglut2 cases (Figure 5m1–2; Figure 12c–f), light labeling in FoxP2 cases, and none in Pdyn cases. Besides this, heavy projections to other thalamic nuclei arose largely from Vglut2 neurons that lack FoxP2 and Pdyn.

Among Vglut2 cases, the most rostral, dorsal injection (0017) produced moderately dense labeling in the mediodorsal (MD), intermediodorsal (IMD), and paracentral (PC) thalamic nuclei. In contrast, injections centered in the medial PB (1280, 0147) produced much heavier labeling in the CM and paracentral (PC) thalamic nuclei, but lighter labeling in MD and IMD (Figure 12c–d).

These Vglut2 cases also had dense labeling in the parvicellular part of the ventral posterior nucleus (VPpc, Figure 5j1–n1), sharply contrasting the absence of labeling here in 0017 (Figure 12e–f). VPpc also contained dense labeling after an injection in the lateral PB (1281), despite less-dense labeling in CM and substantially less labeling in PF. Within the VPpc, its lateral aspect contained distinctively large boutons, similar to those in the PC rostral to it. This lateral aspect of the VPpc was one of only two brain regions with denser labeling on the contralateral side, but only after injections that involved PBeL (cases 1280 and 1281), as noted previously in rats (Bester et al., 1999; Karimnamazi & Travers, 1998; Yasui et al., 1989). Pdyn cases had no labeling in this region of the thalamus, and the light labeling of PF in FoxP2 cases avoided the VPpc entirely, similar to Vglut2 case 0017 (Figure 12g).

Dorsal to these heavily labeled thalamic nuclei, several Vglut2 cases had moderately dense labeling in the IMD, beneath the PVT. Caudally, labeling in the VPpc extended laterally, through the subparafasicular nucleus (Figure 5n1) to the ventromedial border of the MGN and dorsally, into the posterior triangular thalamic nucleus. The ventromedial thalamic nucleus contained Syp-mCherry labeling in all Vglut2 cases. Further caudally, light also labeling appeared in an ill-defined zone just medial to the lateral geniculate nucleus, though the lateral geniculate nucleus itself contained no labeling. Some Vglut2, and to a lesser extent FoxP2 cases did have labeling in the MGN. MGN labeling was more prominent after injections that transduced neurons dorsally, in the inferior colliculus, which is known to provide direct projections to the MGN (Kudo & Niimi, 1978; Ledoux et al., 1987). No Pdyn cases had labeling in the MGN.

Midbrain.

All Vglut2 cases had extensive Syp-mCherry labeling across a variety of midbrain regions. FoxP2 and Pdyn cases contained substantially less labeling in the midbrain, but had qualitatively similar patterns of labeling in the periaqueductal gray matter (PAG) and in a continuum of regions extending rostrally and ventrally from the PB, through the retrorubral field.

In all Vglut2 cases, a broad swath of dense labeling extended medially and rostrally from the PB. Syp-mCherry-labeled axons and boutons extended through the pedunculopontine tegmental nucleus and midbrain reticular formation to reach the PAG (Figure 5o1–s1). At the rostral, dorsolateral extent of this massive terminal field, we found a strikingly dense

terminal field in the lateral superior colliculus, concentrated in the lateral aspect of its deep layers, near the midbrain surface (SC-Lat; Figure 5o1–q1; Figure 13a). All Vglut2 cases had a dense labeling here. Only two FoxP2 cases had light labeling in the SC-Lat and Pdyn cases had no labeling in this region. In the lateral-most Vglut2 injection site (1281), a more diffuse terminal field extended medially through a larger expanse of the SC (not shown).

In Vglut2 cases, a ventral region known as the parabrachial pigmented substance – between the interpeduncular nucleus (IPN) and red nucleus, along the medial lemniscus – contained a moderately dense terminal field of Syp-mCherry-labeled boutons (Figure 5o1; Figure 13a). This terminal field extended through the ventral tegmental area (VTA) and laterally into the substantia nigra pars compacta (SNc) then dorsally and caudally into the retrorubral field, including the A8 cell group. A dense band of boutons atop the IPN bridged the left and right VTA. Atop the medial lemniscus, the dorsal VTA region contained very dense labeling and stood out as one of only two brain regions with denser Syp-mCherry labeling on the contralateral side (the other being the lateral aspect of the VPpc, above). This dense terminal zone may correspond to rostral “tail of the VTA” (Perrotti et al., 2005), and was contiguous bilaterally with Syp-mCherry labeling that extended caudally and dorsally through the rostromedial tegmental nuclei (RMTg; Jhou et al., 2009) to the decussation of the superior cerebellar peduncle (dscp; Figure 5p1–q1; Figure 13b–d). Only light or trace labeling was present in these regions in FoxP2 and Pdyn cases (Figure 5o2–q3).

Along the midline, all cases also contained some labeling in several raphe nuclei, including the dorsal raphe (DR), median raphe, central linear raphe, and rostral linear raphe. Labeling in the raphe nuclei was modestly dense in all Vglut2 cases, much lighter in FoxP2 cases, and minimal in Pdyn cases.

In all FoxP2 and Pdyn cases, the midbrain region that received the most labeling was the PAG. Labeling was densest in its ventrolateral subdivision (PAGvL; Figure 5n1–s3; Figure 13e). The density of labeling in the PAG was qualitatively similar in FoxP2 and Pdyn cases, with a bouton density even denser in two Pdyn cases (1814 and 1812) than in any of the FoxP2 cases. Here again, labeling was still denser in Vglut2 cases, along with extensive, moderately dense labeling in the rostral PAG and throughout the ventral half of the PAG (including DR and PAGvL). Vglut2 cases had variable patterns of labeling in the two dorsal PAG subdivisions (moderately dense in 0017 and 1281, intermediate in 0147, and light in 1280; Figure 13f–g).

Also, unexpectedly, we found dense Syp-mCherry labeling in the ventricular ependymal lining along the cerebral aqueduct in Vglut2 cases (Figure 13h). This was not present in any FoxP2 or Pdyn cases. These labeled boutons encrusted the ventral aqueductal ependyma, along the full length of the cerebral aqueduct, tapering where it meets the third and fourth ventricles. Aqueductal labeling was most prominent in case 1280, where Syp-mCherry-labeled boutons appeared to insert between many ependymal cells. An intermediate density of labeling was present here in 0147, with lighter labeling in 0017. Case 1281 had light labeling throughout the full circumference of the aqueduct, while other cases lacked boutons along the dorsal one-third of the ependyma. None of these cases had any labeled boutons in any other ependymal region or in the subcommissural organ or choroid plexus.

Cerebellum.

The cerebellum does not appear to receive input from the PB. No Pdyn cases had Syp-mCherry labeling anywhere in the cerebellum. One FoxP2 case (0610) had light Syp-mCherry labeling in a small subregion of the interposed nucleus and trace labeling in the flocculus, but in this case, a small number of intrinsic cerebellar neurons expressed Syp-mCherry at the dorsal fringe of the injection site (Supplemental Figure) and in the medial vestibular nucleus. The other three FoxP2 injections did not transduce any neurons in the cerebellum or vestibular nuclei, and these cases had no Syp-mCherry-labeled boutons anywhere in the cerebellum. No Vglut2 cases had neuronal transduction inside the cerebellum, but all four had some labeled neurons immediately caudal to the PB (in the medial vestibular nucleus) and all had trace, grainy Syp-mCherry labeling in deep cerebellar nuclei or scattered mossy fibers in the flocculus or vermis. We cannot exclude the possibility that some PB neurons project very lightly to the cerebellum, but tracing studies in rats and mice indicate that direct projections from this region of the brainstem arise from the superior and medial vestibular nuclei, not the PB (Ando et al., 2020; Ruigrok, 2003).

Hindbrain.

The PB and nuclei immediately surrounding it contained profuse, fibrous labeling that is too dense to classify definitively as axonal or dendritic, particularly in Vglut2 cases. In the hindbrain caudal to the PB, all Vglut2 cases contained widespread, moderately dense labeling throughout the reticular formation. In each case, this continuous field of Syp-mCherry-labeled boutons in the reticular formation was the most prominent labeling in the hindbrain. Labeling in the reticular formation was denser overall in the intermediate reticular nucleus (IRN) than in the parvicellular and gigantocellular reticular nuclei (Figure 5u1–aa1). This broad terminal field extended continuously into the facial nucleus and through the ventrolateral medulla (VLM), which contained a moderately dense field of labeled boutons excluding the compact formation of the nucleus ambiguus (NAc, Figure 5x1). Dorsally, the nucleus of the solitary tract (NTS) contained light, scattered labeling in Vglut2 cases and rarely more than trace labeling in FoxP2 and Pdyn cases. Ventrally, the far-caudal part of the VLM that contains the A1 group and caudal pressor area (CPA) was the only hindbrain region with a density of labeling in some FoxP2 cases (1404 and 1405) that approximated the density in Vglut2 cases. Two Pdyn cases (1812 and 1814) had light labeling here.

Also, as in the midbrain, all raphe nuclei in the hindbrain (magnus, pallidus, and obscurus) contained moderately dense labeling in all Vglut2 cases. Several cranial motor nuclei (trigeminal, facial, and hypoglossal) contained variably dense Syp-mCherry-labeled boutons in all Vglut2 cases, and light labeling in a subset of FoxP2 cases. These cranial motor nuclei contained no labeling in Pdyn cases. Several other hindbrain nuclei in Vglut2 (and to a much lesser extent, FoxP2) cases had a variable number of Syp-mCherry-labeled boutons (see Figure 6). In contrast, Pdyn cases had virtually no labeling throughout the hindbrain, except as mentioned above.

Pathways from the PB to the forebrain.

Descending axons from the PB project around and through the motor trigeminal nucleus and through the reticular formation to reach the hindbrain targets just described. In contrast, ascending projections from the PB follow one of three primary trajectories (Figure 14).

First, most axons projecting to the thalamus (except for the PVT), basal forebrain, amygdala, and cerebral cortex travel through the central tegmental tract (ctt). The ctt is located just lateral to the oculomotor nuclei, between the PAG and red nucleus, and carries the dorsal noradrenergic bundle and other fiber tracts through the midbrain (Ungerstedt, 1971). In all Vglut2 cases, the ctt contained many fascicles of Syp-mCherry-labeled axons. In contrast, the ctt was never labeled in FoxP2 and Pdyn cases, indicating that projections through this tract arise exclusively from non-FoxP2/non-Pdyn neurons in the PB region. Labeled axons in the ctt first produced heavy terminal fields in the caudal thalamus, then turned ventrally through the medial lemniscus and ventromedial thalamic nucleus, then rostrally through the entopeduncular nucleus, to produce heavy terminal fields in the amygdala and basal forebrain. Labeled axons continued through the amygdala and into the external capsule, where they turned caudally, to reach the entorhinal cortex, or dorsally, to reach the insular cortex. Many axons in the external capsule continued past the insular cortex dorsally and rostrally, arcing through the dorsolateral prefrontal cortex and into the frontal pole. Subcortically, axons in the basal forebrain extended rostrally and medially through the sublenticular substantia innominata to produce terminal fields in the BST, nucleus accumbens, septum, and medial prefrontal cortex. A subset of axons running through the septum and medial prefrontal cortex appeared to merge with axons from the dorsolateral prefrontal cortex.

Second, most axonal projections to the hypothalamus travel through the midbrain in a separate, ventral pathway that corresponds roughly to the location of the ventral noradrenergic bundle (Sawchenko & Swanson, 1982; Ungerstedt, 1971). This ventral pathway contained many labeled axons in all FoxP2 and Pdyn cases. It coursed through the A8 region, then turned ventrally and medially to run alongside the medial lemniscus, before merging rostrally into the medial forebrain bundle. These axons continued rostrally through the LHA, emitting axons medially to produce heavy terminal fields in the hypothalamic and preoptic nuclei described above. The light axonal projections to the BST, nucleus accumbens shell, and lateral septum in FoxP2 and Pdyn cases appeared to arise partly from this pathway.

Third, a sizeable minority of labeled axons in all cases projected through a periventricular pathway running along the cerebral aqueduct and beneath the dorsal third ventricle. Just rostral to the PB, these axons separated from the ventral pathway, turning dorsomedially through the midbrain reticular formation to ramify in the PAG. Many of these continued rostrally through the full length of the PAG, then at the midbrain-diencephalic junction a minority turned ventrally to merge with terminal fields in the hypothalamus. The remaining axons emerging from the rostral PAG continued rostrally, through the dorsal thalamus, producing a terminal field throughout the full length of the PVT. Just rostral to the anterior PVT, the few remaining axons in this periventricular pathway either turned dorsally to produce light terminal fields in the lamina terminalis or merged ventrally, contributing to the

dense terminal field in the median preoptic nucleus. In FoxP2 and Pdyn cases, it was difficult to determine the extent to which the light terminal fields in the BST and caudal nucleus accumbens arose from rostral branches of these periventricular axons, relative to the ventral pathway, and both may contribute.

Another relevant feature of PB projections to the forebrain is that many axons from the first two pathways crossed (right to left) through the supraoptic commissure in the ventral hypothalamus, en route to a similar set of targets on the contralateral side. Axons from the ctt and ventral pathway reached the supraoptic commissure through the LHA, crossed to the contralateral hypothalamus at roughly the level of the caudal PVH, and then traveled long distances rostrally or caudally to reach a set of contralateral target sites mirroring the ipsilateral regions shown and described above.

Axonal architecture.

In FoxP2 and Pdyn cases, the morphology of Syp-mCherry-labeled boutons was highly similar in all brain regions. Most were small, with a uniformly grainy appearance. A large majority of labeled boutons in Vglut2 cases had a similarly uniform, grainy morphology.

However, some terminal fields in Vglut2 cases exhibited strikingly different morphologies. One region with distinctive Syp-mCherry labeling was the infralimbic area of the medial prefrontal cortex, where linear concentrations of boutons appeared to encrust apical dendrites, extending medially from layer 5 toward the molecular layer (Figure 15a). A strikingly different pattern was evident in the septum, where peri-somatic boutons clustered so densely as to reveal the shapes of individual neurons and their proximal dendrites (Figure 15b). Terminal fields in the oval BST and lateral capsular CeA exhibited yet another distinctive morphology, with boutons forming tight, peri-somatic rings (Figure 15d–d). In the thalamus, most regions including the medial VPpc and overlying PF contained terminal fields with the uniformly small, grainy boutons found in most PB target sites (Figure 15g). In sharp contrast, we found many giant boutons, up to 5–10 μm long, in the lateral aspect of the VPpc (Figure 15f–g), as noted previously in rats (Bester et al., 1999), and similarly massive boutons rostrally, in the PC (Figure 15e).

Discussion

The PB influences a diverse set of brain structures. Here, we show that all known targets of the PB receive axonal projections from glutamatergic neurons in this brainstem region, while identifying several new targets, including the entorhinal cortex and lateral superior colliculus. We also show that the genetic identity of PB neurons determines which ascending tracts their axons follow and which brain regions they target. PB neurons that express FoxP2 or Pdyn do not project axons through the central tegmental tract and do not target the cerebral cortex, basal forebrain, or amygdala; instead, they target subregions of the diencephalon and brainstem. After discussing limitations of our tracing strategy, we highlight salient differences between the projection patterns of FoxP2 and Pdyn neurons, relative to other glutamatergic neurons in the PB region. We also discuss novel findings, including our identification of sites that may relay information from the PB to the hippocampus.

Limitations.

Viral delivery and Cre-conditional expression of a synaptically targeted protein holds considerable advantages over previous techniques for anterograde axonal tracing. However, as with conventional techniques, interpreting the results is subject to several important considerations. Syp-mCherry has unprecedented sensitivity and specificity as an anterograde marker because, unlike protein tracers that distribute evenly throughout the axoplasm, or fluorescent protein conjugates that insert uniformly throughout the axonal membrane, it is trafficked to presynaptic boutons. This results in punctate labeling that localizes predominantly to presynaptic boutons, but to get there, Syp-mCherry must travel through the axon shaft, so a small amount of labeling along the axon shaft is unavoidable. Therefore, despite highly enriched labeling of presynaptic boutons, a small fraction of labeling may represent Syp-mCherry in axoplasm oriented perpendicular to the plane of section. For any individual bouton in a particular region, confirming that it forms a structural synapse would require immunoelectron microscopy (Wouterlood & Jorritsma-Byham, 1993), and testing whether it forms a functional synapse would require patch-clamp electrophysiology (Petreanu et al., 2007), neither of which are practical at the scale of our study. Instead, we compared the density of Syp-mCherry labeling in brain regions using a semi-quantitative scale (Figure 6). The varied labeling densities and expanses of different brain regions makes it difficult to easily summarize and compare larger, sparsely labeled structures (like the striatum or cerebral cortex) relative to smaller, densely labeled structures (like the reuniens or parastrial nuclei) This approach entails some inherent subjectivity, which we mitigated by referencing the same, consistent standards (Figure 6) to rate the density of labeling in all cases.

Another consideration involves our Cre-conditional approach. Genetic targeting is necessary to study specific subpopulations of PB neurons because their intermingling makes it impossible to stereotaxically target any one subtype in isolation. We used only knockin-Cre strains, in which recombinase expression is driven in tandem with the driver gene, from the endogenous locus. Nonetheless, marker expression in one subpopulation of neurons from a brain region like the PB does not preclude expression of that same gene by unrelated neurons in a neighboring region, as is the case for Vglut2 in the cuneiform nucleus (dorsal to the PB) and pedunculopontine tegmental nucleus (rostral to the PB). Retrograde data from previously published work helps distinguish which projections originate from neurons inside the PB or from neighboring regions (see below), but without complementary retrograde labeling for a given target site it is possible that a particular cluster of labeled puncta might have arisen from virally transduced neurons at the margins of the PB, rather than inside its conventional atlas boundaries. Given the extensively intermingled distributions of PB subpopulations and other neurons rostral and ventromedial to them, genetic distinctions may hold more functional relevance than atlas boundaries in this region. Nonetheless, we refer to the overall Syp-mCherry labeling in this study conservatively, as arising from the PB *region*. Our approach uses recent developmental-genetic information to target neuronal subpopulations in the PB, but future findings may allow us to more selectively identify and target neurons in this intricately complex region.

An additional limitation, which constrains our ability to draw group-wise comparisons across genotypes, is the effect of injection site location on axonal labeling. In addition to genetic identity, the location of labeled neurons within the PB is an important variable influencing the pattern of anterograde labeling (Alden et al., 1994; Bernard et al., 1993; Bester et al., 1997; Bester et al., 1999; Saper & Loewy, 1980; Shin et al., 2011). Because the PB contains a three-dimensional web of intermingled cell types, the ultimate locations and patterns of viral vector spread within each injection site can produce very different labeling patterns despite targeting similar or identical stereotaxic coordinates. For example, we found prominent differences among our Vglut2 cases, with "PB" injection sites that transduced neurons in the rostral, medial, or lateral aspects of this complex labeling divergent projection patterns in the cerebral cortex, hypothalamus, thalamus, STN, and PAG. Among these differences, we identified a massive glutamatergic PB projection to the VMH, which a previous study claimed not to exist (Garfieldet al., 2014). Nonetheless, the VMH was one of the most heavily labeled structures in the brain after an injection centered in the lateral PB (1281), contrasting the lighter labeling there in three other cases. AAV injections in the previous study presumably missed the rostral, dorsal subregion of the lateral PB that contains VMH-projecting neurons (Fulwiler & Saper, 1984, 1985; Grady et al., 2020; Zaborszky et al., 1984). To reduce the odds of false-negative experimental results when stereotaxically delivering viral vectors into the PB region, it is important to consider the location and distribution of transduced neurons within each injection site as an independent variable. Our combined Vglut2 cases transduced neurons in all PB subregions and labeled projections to all known targets of the PB, and more.

Genetic identity determines efferent projection patterns: FoxP2 and Pdyn relative to other PB glutamatergic neurons.

Intermixed PB neurons originate from two, distinct precursor populations in the developing hindbrain (Dai et al., 2008; Gray, 2008; Miller et al., 2012; Rose et al., 2009; Wang et al., 2005). One population originates from *Math1*/*Atoh1*-expressing precursor cells in the rhombic lip, and many of their neuronal progeny in the PB express *Foxp2* postnatally (Geerling et al., 2016; Geerling et al., 2011; Gray, 2008; Miller et al., 2012; Verstegen et al., 2017a). Many of these also express *Pdyn*, which encodes the neuropeptide co-transmitter dynorphin (Geerling et al., 2016; Miller et al., 2012). Thus, *Foxp2* expression is useful for identifying and accessing a large, developmentally distinct subpopulation of PB neurons, within which a further subpopulation expresses *Pdyn*. The functional significance of *Foxp2* or *Pdyn* expression by PB neurons is unknown, and we use these genetic markers to access and study the neurons that express them, not the proteins they encode.

While *Pdyn* is found in a large subset of *Foxp2*-expressing neurons (see Figure 2 and Figure 3p–u), many *Foxp2*-expressing PB neurons lack *Pdyn*, particularly at more rostral levels. There, many *Foxp2*-expressing neurons express a different neuropeptide gene, *Cck* (Garfield et al., 2014). These *Cck*-expressing neurons project their axons to the VMH (Fulwiler & Saper, 1985; Garfield et al., 2014; Zaborszky et al., 1984), and presumably account for the Syp-mCherry labeling that was present in the VMH in our FoxP2, but not Pdyn cases. *Cck* is also expressed in neurons that lack FoxP2, including a caudal cluster in the medial PB that projects axons heavily to the insular cortex (Grady et al., 2020).

The FoxP2 projection to the VMH, which was absent in all Pdyn cases, was the most prominent difference between our FoxP2 and Pdyn cases. We were surprised to find so little contrast, overall, between the efferent projection patterns of FoxP2 and Pdyn neurons. Besides the VMH, we found only a handful of minor discrepancies, primarily in the brainstem. For example, the lateral superior colliculus in the midbrain and cranial motor nuclei in the hindbrain contained light Syp-mCherry labeling in FoxP2 cases, but little or no labeling in Pdyn cases. Besides these few, small differences, a key finding of our study is that the subset of FoxP2 neurons that expresses *Pdyn* appears to deliver information to a set of target sites that is largely similar to the projection targets of the overall population of FoxP2 neurons in the PB region.

When comparing the efferent projections of FoxP2 and Pdyn cases with the larger set of PB projections in Vglut2 cases, it is simpler to mention the subset of target regions that do receive input, rather than the longer list of those that do not. Nonetheless, a few salient absences are worth highlighting. For example, axonal projections in FoxP2 and Pdyn cases avoid the central tegmental tract entirely. Also, their boutons are uniformly grainy in appearance, without any of the other morphologies shown in Figure 14. Further, *Foxp2*- and *Pdyn*-expressing neurons send virtually no output to the cerebral cortex, basal forebrain, amygdala, or VPpc, and project fewer axons to the hindbrain. The molecular subtypes of PB neurons that *do* project axons to these brain regions are topics of on-going investigation. Several PB subpopulations do not express *Foxp2* or *Pdyn*, including the cortically projecting, *Cck*-expressing subset mentioned above (Grady et al., 2020). One of these subpopulations expresses the neuropeptide gene *Calca*, and projects axons to a subset of the targets in our Vglut2 cases (particularly 1281) that largely complement those labeled in our FoxP2 and Pdyn cases (see Supplemental Figure 6 of Chen et al., 2018). It will be important to determine which subpopulations supply the remaining PB projections to the hindbrain and other sites listed above. Of course, some of the projections labeled in Vglut2, but not FoxP2/Pdyn cases could originate from neurons located just outside the PB. For example, the moderately dense projections to hindbrain oromotor nuclei may originate ventral to the PB, from neurons in the Kölliker-Fuse nucleus or supratrigeminal region (Travers & Norgren, 1983).

Shifting attention back to FoxP2 and Pdyn neurons, their efferent projections account for a majority of the glutamatergic PB output to the preoptic area and hypothalamus. They also represent a substantial subset of PB projections to the PVT and PAG, with lighter contributions to several other nuclei, including the xiphoid, reuniens, and intermediodorsal thalamic nuclei. This pattern complements a previous study, which used conventional anterograde tracing from the PB/pre-LC region and then retrograde tracer injections in many brain regions followed by FoxP2 immunolabeling to identify target regions that receive input from PB neurons with FoxP2 nuclear immunoreactivity in rats (Shin et al., 2011).

Two other studies in mice, published during the preparation of our manuscript, delivered Cre-conditional vectors to the PB region in *Pdyn-IRES-Cre* mice to label axonal projections that are partly consistent with our findings (see Extended Data Fig. 8 of both Kim et al., 2020; Lee et al., 2019). In our Pdyn cases, injection sites that did (1812) or did not (1813, 1814) transduce pre-LC neurons produced Syp-mCherry labeling in a virtually identical set

of target regions. However, the images shown by Lee et al. after targeting the pre-LC did not include any labeling in the MnPO, VLPO, PSTN, Re/Rh/Xi, PAG, caudal VLM, and other target areas identified in our study. Our use of immunohistochemical labeling and whole-slide scanning may have offered better sensitivity, and Nissl counterstaining in our study may have allowed more precise cytoarchitectural distinctions, for example between dense labeling in the parastrial preoptic nucleus, which may have been mis-interpreted as "vBNST" (Lee et al., 2019).

The functional roles of *Pdyn*-expressing FoxP2 neurons are beginning to come into focus. First, we identified a functional link to sodium appetite in rats by showing that FoxP2+ neurons in the pre-LC (along with a smaller subset of FoxP2+ lateral PB neurons) receive input from aldosterone-sensitive neurons in the NTS and are co-activated during sodium appetite (Geerling & Loewy, 2007; Geerling et al., 2011). These findings were confirmed and extended in mice (Jarvie & Palmiter, 2017; Resch et al., 2017), and more recent experiments suggest that *Pdyn*-expressing neurons in the pre-LC may help generate sodium appetite and may receive inhibitory input from the BST when salt is consumed (Lee et al., 2019). Separately, two clusters of lateral PB neurons relay either warm or cool skin temperature information from the spinal cord to the hypothalamus (Nakamura & Morrison, 2008, 2010). We found that neurons in both populations ubiquitously express FoxP2 and that a *Pdyn*-expressing subset in the dorsal lateral PB subnucleus (PBdL) is warm-activated (Geerling et al., 2016). Thus, changes in ambient temperature are sensed by warm and cool thermosensory axons in the skin, signaled through spinoparabrachial axons, and then relayed rostrally by *Pdyn*− (cool-relay) and *Pdyn*+ (warm-relay) subsets. These neurons are probably responsible for PB-dependent responses that are necessary for autonomic and behavioral thermoregulation (Nakamura & Morrison, 2008, 2010; Yahiro et al., 2017). Interspersed between the warm-relay *Pdyn* neurons (in PBdL) and the medial, sodium-deprivation-activated *Pdyn* neurons (in pre-LC) is another population of *Pdyn* neurons that relay visceral, mechanosensory signals important for meal termination (Kim et al., 2020). Other studies indicate that a subset of Pdyn neurons in PBdL relay pain signals (Chiang et al., 2020; Hermanson, Telkov, et al., 1998). One of these studies, published during the preparation of our manuscript, claimed that *Pdyn* neurons relay noxious signals from the spinal cord to neighboring, amygdala-projecting neurons in PBeL (Chiang et al., 2020), though it is unclear whether the labeled processes in question (YFP-labeled fibers extending ventrolaterally from PBdL) are dendrites or axons, or whether they form synaptic contact with any neurons in PBeL.

We lack markers to differentiate these functionally distinct *Pdyn* subpopulations. Besides these, there are at least two other, non-*Pdyn* subpopulations of FoxP2 neurons in the PB: the cool-relay cluster in PBreL that projects axons to the preoptic area (Geerling et al., 2016) and *Cck*-expressing neurons in the superior lateral PB neurons that project to the VMH (Garfield et al., 2014; Grady et al., 2020).

Comparison with previous tracing studies.

The general pattern of efferent projections in our Vglut2 cases is largely consistent with the pivotal anterograde tracing study of Saper and Loewy (1980). After delivering tritiated

amino acids into the PB region, they traced efferent projections from injection sites centered in either the medial or lateral PB subdivision. Their results extended the findings of Norgren, who had used axonal degeneration and anterograde autoradiography to trace efferent projections emerging from the caudal, gustatory PB ("pontine taste area"; Norgren, 1976; Norgren & Leonard, 1971, 1973).

The overall set of brain regions that receive glutamatergic, Syp-mCherry-labeled boutons in our study includes all the efferent projection targets identified in these original studies, and those identified in subsequent studies using other anterograde tracers, including wheat germ agglutinin-horseradish peroxidase, biotinylated dextran amine, or *Phaseolus vulgaris* leukoagglutinin (PHA-L) (Alden et al., 1994; Bernard et al., 1993; Bester et al., 1997; Bester et al., 1999; Bianchi et al., 1998; Hayakawa et al., 1999; Herbert et al., 1990; Karimnamazi & Travers, 1998; Krukoff et al., 1993; Shin et al., 2011; Thompson & Swanson, 1998). Complementary, retrograde tracing experiments in several additional studies confirmed that neurons within the PB, rather than in surrounding structures, project axons to these target sites (Fulwiler & Saper, 1984; Herbert et al., 1990; Shin et al., 2011; Tokita et al., 2010). Listing all the minor differences among these prior tracing studies, or between their results and ours, would be well beyond the scope of this Discussion. However, two categories of new observations in our study require further consideration.

First, for several brain regions receiving input from the PB *region*, previous retrograde tracing results clearly showed that the projection originates outside or at the margins of the PB. These include: (a) the MGN, which receives direct axonal projections from the inferior colliculus (Kudo & Niimi, 1978; Ledoux et al., 1987), which contained virally transduced neurons at the dorsal aspect of several of our injection sites; (b) the STN, which receives direct projections from neurons in the PPN, rostral to the PB (Canteras et al., 1990; Jackson & Crossman, 1983); and (c) the flocculus, lobule X, and deep nuclei of the cerebellum, which receive input from neurons in the vestibular nuclei along the caudal, ventral and medial borders of the PB (Ando et al., 2020; Ruigrok, 2003).

Second, we identified targets that were not highlighted in previous PB tracing studies, despite retrograde labeling of PB neurons in other tracing studies that focused on afferents to the brain region in question. In contrast to previous reports of PB axonal projections to the posterior basolateral amygdaloid nucleus in rats (BLP; Bernard et al., 1993; Saper & Loewy, 1980), in our cases Syp-mCherry punctae concentrated in the APir, a transitional allocortex (also called the post-piriform transition area, or "TR"; Dong, 2008) that lies ventrolateral and slightly caudal to the BLP in mice. While this could represent a species difference, axonal labeling in previous illustrations (see for example Figure 3F of Saper & Loewy, 1980) is in a location more consistent with the homologous transition cortex in rats, which was later delineated and named "TR" (Swanson, 1992) or "APir" (Paxinos & Watson, 2007). Consistent with our interpretation, injecting a retrograde tracer into this cortical region in rats labeled neurons in the PB (Santiago & Shammah-Lagnado, 2005).

Across the piriform cortex from the APir, we also discovered a Vglut2 terminal field concentrated over layer 5 of the rostral entorhinal cortex. To our knowledge, this projection was not reported in any PB efferent tracing studies, although we are aware of one example in

which light labeling of PB neurons after a retrograde tracer injection in Ent had been dismissed as more likely representing projections to a bordering area (Santiago & Shammah-Lagnado, 2005).

Another unexpected target that receives substantial input from the PB region is the lateral extent of the deep layers of the superior colliculus (SC-Lat). We are not aware of any previous descriptions of this dense, concentrated projection to SC-Lat, but one panel in a previous study included a light, scattered projection across the ipsilateral SC after an anterograde tracer injection into the lateral PB (Figure 3I of Saper & Loewy, 1980), similar to the light, broader projection to the SC we observed in case 1281. This broader projection may originate, in part, from neurons immediately rostral to the lateral PB, in the parabigeminal nucleus or nucleus of the lateral lemniscus (Graybiel, 1978; Taylor et al., 1986). However, the injection sites in our three Vglut2 cases with dense labeling in SC-Lat did not approach those nuclei. A complementary finding that tracer injections into the SC produced retrograde labeling of PB neurons in cats (Edwards et al., 1979) confirms that at least some input to SC-Lat originates in the PB. It is tempting to speculate a role in attention, orienting responses, oculomotor control, REM-sleep-related eye movements, or even eyelid opening, but the function of this projection remains unknown. From a neuroanatomical perspective, unraveling its function would benefit from using retrograde tracing in mice to begin characterizing the source neurons in or near the PB.

Yet another new observation in our study is that in the ventral midbrain, a large, bilateral subset of Syp-mCherry boutons targets a paramedian region known as the “tail of the VTA” or RMTg. This region contains GABAergic neurons that are activated by dopamine reuptake inhibitors and that serve as an inhibitory relay to dopaminergic neurons in the underlying VTA and SNc (Jhou et al., 2009; Perrotti et al., 2005). A previous tracing study described projections to this ventral, paramedian region of the midbrain (Saper & Loewy, 1980), and retrograde tracer injections into the RMTg labeled many neurons in the PB (Jhou et al., 2009). This projection likely underlies the PB-dependent, short-latency inhibition of midbrain dopaminergic neurons in response to noxious stimuli (Coizet et al., 2010), which appear to operate in parallel with PB projections that relay viscerosensory signals and directly excite dopaminergic neurons (Han et al., 2018).

Novel functional perspectives.

Many authors have contemplated the functional roles of projections from the PB to specific target regions. These include: regulating body temperature in the preoptic area and hypothalamus (Geerling et al., 2016; Nakamura & Morrison, 2008, 2010); influencing attention or arousal through the hypothalamus, thalamus, amygdala, basal forebrain, or cerebral cortex (Chou et al., 2002; Fuller et al., 2011; Kaur et al., 2013; Kaur et al., 2017; Qiu et al., 2016; Saper, 1982; Saper & Loewy, 1980); relaying danger signals to a variety of brain regions (Campos et al., 2018; Chiang et al., 2019; Palmiter, 2018; Saper, 2016); inhibiting food, salt, and water intake in the CeA or hypothalamus (Carter et al., 2015; Carter et al., 2013; Kim et al., 2020; Park et al., 2020; Ryan et al., 2017); and modulating autonomic function in the hindbrain, hypothalamus, CeA, or BST (Chamberlin & Saper, 1992, 1994; Davern, 2014; Saper & Loewy, 1980; Yokota et al., 2015). For the most part, we

will reserve discussion of brain regions not innervated by FoxP2 or Pdyn neurons for future publications focusing on the PB subpopulations that do target those regions, but here we will highlight three functionally relevant observations derived from our new neuroanatomical data.

First, PB projections to the hypothalamus are abundant and complex, as reviewed in previous work (Bester et al., 1997; Fulwiler & Saper, 1984). Among these patterns, we find a major distinction between glutamatergic subpopulations. Specifically, neurons that express Vglut2, and to a lesser extent (non-*Pdyn*-expressing) FoxP2 neurons, project massively to the VMH. In striking contrast, the VMH was empty in Pdyn cases, despite their similarly dense terminal fields in other hypothalamic regions, prominently including the LHA "orexin field." Our findings complement previous evidence that rostral PB neurons that express *Cck*, a subset of which express FoxP2, project heavily to the VMH and other hypothalamic nuclei (Fulwiler & Saper, 1985; Garfield et al., 2014; Hermanson, Larhammar, et al., 1998) by adding that *Pdyn*-expressing neurons located caudally project heavily to the LHA, not the VMH. PB neurons that project axons to the VMH are activated by noxious, spino-parabrachial inputs (Bester et al., 1995; Hermanson, Larhammar, et al., 1998), and neurons in the VMH drive stereotyped aggressive and sometimes sexual behaviors (Lee et al., 2014; Lin et al., 2011; Yang et al., 2013). Thus, a subset of glutamatergic PB neurons (some of which express FoxP2) provides copious input to the VMH, which likely triggers defensive or aggressive affective states in response to painful stimuli. *Pdyn*-expressing glutamatergic PB neurons do not participate in this pathway, and may instead drive autonomic, metabolic, appetitive, or aversive behavioral effects that are mediated by preoptic nuclei, LHA orexin neurons, and other hypothalamic nuclei.

Next, existing discussions of the PB either ignored the thalamus or focused primarily on its relay function as delivering gustatory and other sensory information to the so-called gustatory or viscerosensory thalamus (VPpc) (Bester et al., 1999; Fulwiler & Saper, 1984; Norgren & Leonard, 1973). However, the PB probably conveys a broader range of information than just this, and it certainly projects it to a wider set of thalamic nuclei (Bester et al., 1999; Krout & Loewy, 2000). We show that non-*Pdyn*-expressing, glutamatergic neurons densely target several parts of the thalamus, particularly the intralaminar nuclei PF and CM, which are known to send massive axonal projections to the dorsal striatum and prefrontal cortex (Van der Werf et al., 2002). *Pdyn*-expressing neurons contribute to the larger set of PB projections targeting the full extent of the PVT, which projects to the ventral striatum, as well as Re and Rh, which in turn target the prefrontal cortex and hippocampus. The function of PB input to these thalamic nuclei is unknown, but we speculate that they convey painful and/or other (pruritic, thermal, gustatory, other viscerosensory) stimuli that increase the gain of somatomotor activation (via broad excitatory output to the striatum) and of cortical-limbic networks subserving arousal and attention (via broad excitatory output to prefrontal cortex). Consistent with the latter possibility, a minority of ischemic strokes in the thalamus impair arousal, and this finding correlates with a posterior location, centered in or near the human CM and PF (Hindman et al., 2018). Further, rodent experiments demonstrated an arousal-promoting role for both PVT and CM/PF (Gent et al., 2018; Ren et al., 2018).

Finally, midline projections to the Re, Rh, and Xi stand apart from this pattern because these thalamic nuclei send output directly to the hippocampus (Van der Werf et al., 2002). This suggests that a subset of PB efferent projections may influence spatial navigation, or semantic and episodic memory encoding (Burgess et al., 2002). We identified several additional brain regions, outside the thalamus, that receive input from the PB and project axons directly to the hippocampus. These include the rostral entorhinal cortex, amygdalopiriform transition cortex, lateral septum, and septohippocampal nucleus, each of which represents a potential route for PB-relayed information to influence hippocampal memory circuits. The nature of the information relayed from the PB to the hippocampus is unknown, and it is unclear how this excitatory input would interact with the better-known sets of information flowing into the hippocampus from association cortices and other afferents. Given the imprecise nature of most viscerosensory and noxious information relayed by PB neurons, it is possible that they supply contextual information to enhance the salience of or increase the likelihood of encoding memories, rather than delivering the primary information to be encoded as a memory engram.

Conclusion.

Our results show that the genetic identity of PB neurons determines their connectivity (and therefore, function). The method and results presented here provide a new framework for mapping the efferent projections of PB neurons based on their intrinsic genetic identity, rather than by grouping PB neurons based their location and cytoarchitectural appearance. Beyond improving the consistency of future experimental and ontological work across laboratories that study mice, the larger aim of this approach is that classifying PB neurons and their connections using genetic markers and cell-type-specific labeling will enhance the translation of basic science discoveries in experimental animals to the brains of our primary species of interest – the human.

Supplementary Material

Refer to Web version on PubMed Central for supplementary material.

Role of Authors

JCG planned experiments; LP performed all stereotaxic injections; LP, JCG, FSG, and DH performed histologic staining and slide-scanning microscopy; DH, FSG, and JCG planned the analysis; FSG developed and applied the algorithm for semi-automated identification and plotting of boutons; DH and JCG analyzed data and wrote the manuscript; DH drafted and edited all figures with JCG; JCG supervised the project. All authors reviewed and discussed the results and contributed to the final manuscript.

Other Acknowledgements

Gabrielle Iverson assisted with histology, including *in situ* hybridization. Alison Hsu and Erica Hsu manually plotted immunolabeled boutons used to train the machine learning algorithm. We thank Richard Palmiter for sharing *Foxp2-IRES-Cre* mice, Jadylin Tolda and Frederico Fazan for proofreading the manuscript, Silvia Gasparini for assistance with confocal microscopy, and Clifford Saper for mentorship and constructive criticisms.

Grant sponsors:

NIH K08 NS099425 (JCG)

List of Abbreviations

AAA	anterior amygdaloid area
ac	anterior commissure
AcbSh	accumbens nucleus, shell
AHA	anterior hypothalamic area
AI	agranular (ventral) insular cortex
AON	anterior olfactory nucleus
AP	area postrema
APir	amygdalopiriform transition area
APN	anterior pretectal nucleus
Aq	cerebral aqueduct
Arc	arcuate hypothalamic nucleus
BLA	basolateral amygdalar nucleus
BMA	basomedial amygdalar nucleus
BST	bed nucleus of the stria terminalis
BSTal	BST anterolateral subnucleus
BSTfu	BST fusiform subnucleus
BSTov	BST oval subnucleus
BSTp	BST posterior subdivision
BSTvL	BST ventrolateral subdivision
CeA	central amygdalar nucleus
CeAc	CeA, (lateral) capsular subdivision
CeAl	CeA, lateral subdivision
CeAm	CeA, medial subdivision
Cb	cerebellum
Cck	cholecystokinin
Cla	claustrum
CLi	central linear raphe
CM	centromedian thalamic nucleus

CoA	cortical amygdalar area
CPA/A1	caudal pressor area / A1 group
ctt	central tegmental tract
Cun	cuneiform nucleus
DCN	deep cerebellar nuclei
DI	dysgranular (middle) insular cortex
dLPFC	dorsolateral prefrontal cortex
DMH	dorsomedial hypothalamic nucleus
DP	dorsal peduncular cortical area
DR	dorsal raphe
dscp	decussation of the superior cerebellar peduncle
DTN	dorsal tegmental nucleus
Ent	entorhinal cortical area
EPd	endopiriform nucleus, dorsal subdivision
EPi	endopiriform nucleus, intermediate subdivision
EPv	endopiriform nucleus, ventral subdivision
Epy	ependymal cell layer of cerebral aqueduct
EW	Edinger-Westphal nucleus
FL	flocculus of cerebellum
FoxP2	Forkhead box P2
fr	fasciculus retroflexus
GI	granular (dorsal) insular cortex
GiRN	gigantocellular reticular nucleus
GPe	globus pallidus pars externa
GPi	globus pallidus pars interna (entopeduncular)
Hc	hippocampus
IA	intercalated amygdalar nucleus
ic	internal capsule
IC	insular cortical area

IFV	interfascicular trigeminal (CN V) nucleus
IG	induseum griseum
ILA	infralimbic cortical area
IMD	intermediodorsal thalamic nucleus
IO	inferior olivary complex
IPN	interpeduncular nucleus
IRN	intermediate reticular nucleus
Isl	island of Calleja
KF	Kolliker-Fuse nucleus
L6 PFC	layer 6 of the prefrontal cortex
LDT	laterodorsal tegmental nucleus
LGN	lateral geniculate nucleus
LHA	lateral hypothalamic area
LHb	lateral habenular nucleus
LM	lateral mammillary nucleus
LPOA	lateral preoptic area
LRN	lateral reticular nucleus
LS	lateral septum
LSi	LS intermediate subdivision
LSr	LS rostral subdivision
LSv	LS ventral subdivision
MA	magnocellular (basal forebrain) nucleus
MD	mediodorsal thalamic nucleus
MeA	medial amygdalar nucleus
MGN	medial geniculate nucleus
MHb	medial habenular nucleus
ml	medial lemniscus
MM	medial mammillary nucleus
MnPO	median preoptic nucleus

MOB	main olfactory bulb
MPN	medial preoptic nucleus
MPOA	medial preoptic area
MR	median raphe
MRN	midbrain reticular nucleus
MS	medial septum
NAc	nucleus ambiguus, compact formation
NBM	nucleus basalis of Meynert
NDB	nucleus of the diagonal band
NeoCtx	neocortex
NLOT	nucleus of the lateral olfactory tract
NTB	nucleus of trapezoid body
NTS	nucleus of the solitary tract
NTS-lat	NTS lateral subdivision
NTS-med	NTS medial subdivision
oc	optic chiasm
ot	optic tract
OVLT	organum vasculosum of lamina terminalis
PAG	periaqueductal gray matter
PAGdL	PAG dorsolateral subdivision
PAGdm	PAG dorsomedial subdivision
PAGvL	PAG ventrolateral subdivision
PaRN	parvicellular reticular nucleus
PB	parabrachial nuclear complex
PBsL	superior lateral PB subnucleus
PBreL	rostral-to-external Lateral PB subnucleus
PBcL	central lateral PB subnucleus
PBdL	dorsal lateral PB subnucleus
PC	paracentral thalamic nucleus

Pdyn	prodynorphin
periLGN	peri-lateral geniculate nucleus
PeriRh	perirhinal cortical area
PF	parafascicular thalamic nucleus
PH	posterior hypothalamic nucleus
PHA-L	*Phaseolus Vulgaris* leukoagglutinin
PIL	posterior intralaminar thalamic nucleus
Pir	piriform cortex
PL-ACA	prelimbic & anterior cingulate cortex
pre-LC	pre-locus coeruleus
PMd	posterior mammillary nucleus, dorsal
PMv	posterior mammillary nucleus, ventral
Pn	pontine nuclei
PO	posterior thalamic nuclear complex
PoT	posterior triangular thalamic nucleus
PPN	pedunculopontine (tegmental) nucleus
PRN	pontine reticular nucleus
Prt	pretectal area
PS	parastrial nucleus
PSTN	parasubthalamic nucleus
PSV	principal sensory trigeminal (CN V) nucleus
PT	paratenial thalamic nucleus
PVH	paraventricular hypothalamic nucleus
PVT	paraventricular thalamic nucleus
RCA	retrochiasmatic area of the hypothalamus
Re	reuniens thalamic nucleus
Rh	rhomboid thalamic nucleus
rLA	rostral lateral amygdalar nucleus
RLi	rostral linear raphe

RMg	raphe magnus
RMTg	rostromedial tegmental nucleus
RN	red nucleus
ROb	raphe obscurus
RR/A8	retrorubral area / A8 group
SC	superior colliculus
SC-Lat	superior colliculus, lateral aspect
SCN	suprachiasmatic nucleus
SCO	subcommissural organ
scp	superior cerebellar peduncle
SEZ	subependymal germinal zone
SF	septofimbrial nucleus
SFO	subfornical organ
SHi	septohippocampal nucleus
SI	substantia innominata
SNc	substantia nigra, pars compacta
SNr	substantia nigra, pars reticulata
SOA	septal-olfactory area
SOC	superior olivary complex
SON	supraoptic nucleus
SPF	subparafasicular nucleus
SpV	spinal trigeminal nucleus
st	stria terminalis
STN	subthalamic nucleus
Str	striatum
Str/GP bdr	border between striatum and GPe
SUM	supramammillary nucleus
Syp-mCherry	synaptophysin-mCherry
TH	tyrosine hydroxylase

TM	tuberomammillary nucleus
TRN	tegmental reticular nucleus
TT	tenia tecta
Ubc	ubiquitin C
V	trigeminal (CN VI) motor nucleus
Vglut2	vesicular glutamate transporter 2 (*Slc17a6*)
VII	facial (CN VII) motor nucleus
VLPO	ventrolateral preoptic nucleus
VLM	ventrolateral medulla
VM	ventromedial thalamic nucleus
VMH	ventromedial hypothalamic nucleus
VMPO	ventromedial preoptic area
VNC	vestibular nuclear complex
VPpc	parvicellular ventral posterior thalamic nucleus
VTA	ventral tegmental area
Xi	xiphoid thalamic nucleus
XII	hypoglossal (CN XII) motor nucleus
ZI	zona incerta

References

Alden M, Besson JM, & Bernard JF (1994). Organization of the efferent projections from the pontine parabrachial area to the bed nucleus of the stria terminalis and neighboring regions: a PHA-L study in the rat. J Comp Neurol, 341(3), 289–314. 10.1002/cne.903410302 [PubMed: 7515078]

Ando T, Ueda M, Luo Y, & Sugihara I (2020). Heterogeneous vestibulocerebellar mossy fiber projections revealed by single axon reconstruction in the mouse. J Comp Neurol. 10.1002/cne.24853

Bernard JF, Alden M, & Besson JM (1993). The organization of the efferent projections from the pontine parabrachial area to the amygdaloid complex: a Phaseolus vulgaris leucoagglutinin (PHA-L) study in the rat. J Comp Neurol, 329(2), 201–229. 10.1002/cne.903290205 [PubMed: 8454730]

Bernard JF, Dallel R, Raboisson P, Villanueva L, & Le Bars D (1995). Organization of the efferent projections from the spinal cervical enlargement to the parabrachial area and periaqueductal gray: a PHA-L study in the rat. J Comp Neurol, 353(4), 480–505. 10.1002/cne.903530403 [PubMed: 7759612]

Bester H, Besson JM, & Bernard JF (1997). Organization of efferent projections from the parabrachial area to the hypothalamus: a Phaseolus vulgaris-leucoagglutinin study in the rat. J Comp Neurol, 383(3), 245–281. [PubMed: 9205041]

Bester H, Bourgeais L, Villanueva L, Besson JM, & Bernard JF (1999). Differential projections to the intralaminar and gustatory thalamus from the parabrachial area: a PHA-L study in the rat. J Comp Neurol, 405(4), 421–449. [PubMed: 10098938]

Bester H, Menendez L, Besson JM, & Bernard JF (1995). Spino (trigemino) parabrachiohypothalamic pathway: electrophysiological evidence for an involvement in pain processes. J Neurophysiol, 73(2), 568–585. 10.1152/jn.1995.73.2.568 [PubMed: 7760119]

Bianchi R, Corsetti G, Rodella L, Tredici G, & Gioia M (1998). Supraspinal connections and termination patterns of the parabrachial complex determined by the biocytin anterograde tract-tracing technique in the rat. J Anat, 193 (Pt 3), 417–430. 10.1046/j.1469-7580.1998.19330417.x [PubMed: 9877297]

Burgess N, Maguire EA, & O'Keefe J (2002). The human hippocampus and spatial and episodic memory. Neuron, 35(4), 625–641. 10.1016/s0896-6273(02)00830-9 [PubMed: 12194864]

Caggiano V, Leiras R, Goni-Erro H, Masini D, Bellardita C, Bouvier J, Caldeira V, Fisone G, & Kiehn O (2018). Midbrain circuits that set locomotor speed and gait selection. Nature, 553(7689), 455–460. 10.1038/nature25448 [PubMed: 29342142]

Calhoun ME, Jucker M, Martin LJ, Thinakaran G, Price DL, & Mouton PR (1996). Comparative evaluation of synaptophysin-based methods for quantification of synapses. J Neurocytol, 25(12), 821–828. 10.1007/bf02284844 [PubMed: 9023727]

Campos CA, Bowen AJ, Roman CW, & Palmiter RD (2018). Encoding of danger by parabrachial CGRP neurons. Nature, 555(7698), 617–622. 10.1038/nature25511 [PubMed: 29562230]

Canteras NS, Shammah-Lagnado SJ, Silva BA, & Ricardo JA (1990). Afferent connections of the subthalamic nucleus: a combined retrograde and anterograde horseradish peroxidase study in the rat. Brain Res, 513(1), 43–59. 10.1016/0006-8993(90)91087-w [PubMed: 2350684]

Carter ME, Han S, & Palmiter RD (2015). Parabrachial calcitonin gene-related peptide neurons mediate conditioned taste aversion. J Neurosci, 35(11), 4582–4586. 10.1523/JNEUROSCI.3729-14.2015 [PubMed: 25788675]

Carter ME, Soden ME, Zweifel LS, & Palmiter RD (2013). Genetic identification of a neural circuit that suppresses appetite. Nature, 503(7474), 111–114. 10.1038/nature12596 [PubMed: 24121436]

Chamberlin NL, & Saper CB (1992). Topographic organization of cardiovascular responses to electrical and glutamate microstimulation of the parabrachial nucleus in the rat. J Comp Neurol, 326(2), 245–262. 10.1002/cne.903260207 [PubMed: 1362207]

Chamberlin NL, & Saper CB (1994). Topographic organization of respiratory responses to glutamate microstimulation of the parabrachial nucleus in the rat. J Neurosci, 14(11 Pt 1), 6500–6510. [PubMed: 7965054]

Chen JY, Campos CA, Jarvie BC, & Palmiter RD (2018). Parabrachial CGRP Neurons Establish and Sustain Aversive Taste Memories. Neuron, 100(4), 891–899 e895. 10.1016/j.neuron.2018.09.032 [PubMed: 30344042]

Chen MC, Ferrari L, Sacchet MD, Foland-Ross LC, Qiu MH, Gotlib IH, Fuller PM, Arrigoni E, & Lu J (2015). Identification of a direct GABAergic pallidocortical pathway in rodents. Eur J Neurosci, 41(6), 748–759. 10.1111/ejn.12822 [PubMed: 25581560]

Chiang MC, Bowen A, Schier LA, Tupone D, Uddin O, & Heinricher MM (2019). Parabrachial Complex: A Hub for Pain and Aversion. J Neurosci, 39(42), 8225–8230. 10.1523/JNEUROSCI.1162-19.2019 [PubMed: 31619491]

Chiang MC, Nguyen EK, Canto-Bustos M, Papale AE, Oswald AM, & Ross SE (2020). Divergent Neural Pathways Emanating from the Lateral Parabrachial Nucleus Mediate Distinct Components of the Pain Response. Neuron. 10.1016/j.neuron.2020.03.014

Chou TC, Bjorkum AA, Gaus SE, Lu J, Scammell TE, & Saper CB (2002). Afferents to the ventrolateral preoptic nucleus. J Neurosci, 22(3), 977–990. [PubMed: 11826126]

Coizet V, Dommett EJ, Klop EM, Redgrave P, & Overton PG (2010). The parabrachial nucleus is a critical link in the transmission of short latency nociceptive information to midbrain dopaminergic neurons. Neuroscience, 168(1), 263–272. 10.1016/j.neuroscience.2010.03.049 [PubMed: 20363297]

Dai JX, Hu ZL, Shi M, Guo C, & Ding YQ (2008). Postnatal ontogeny of the transcription factor Lmx1b in the mouse central nervous system. J Comp Neurol, 509(4), 341–355. 10.1002/cne.21759 [PubMed: 18512225]

Davern PJ (2014). A role for the lateral parabrachial nucleus in cardiovascular function and fluid homeostasis. Front Physiol, 5, 436 10.3389/fphys.2014.00436 [PubMed: 25477821]

Dong HW (2008). Allen reference atlas : a digital color brain atlas of the C57Black/6J male mouse. Wiley.

Edwards SB, Ginsburgh CL, Henkel CK, & Stein BE (1979). Sources of subcortical projections to the superior colliculus in the cat. J Comp Neurol, 184(2), 309–329. 10.1002/cne.901840207 [PubMed: 762286]

Feil K, & Herbert H (1995). Topographic organization of spinal and trigeminal somatosensory pathways to the rat parabrachial and Kolliker-Fuse nuclei. J Comp Neurol, 353(4), 506–528. 10.1002/cne.903530404 [PubMed: 7759613]

Fuller PM, Sherman D, Pedersen NP, Saper CB, & Lu J (2011). Reassessment of the structural basis of the ascending arousal system. J Comp Neurol, 519(5), 933–956. 10.1002/cne.22559 [PubMed: 21280045]

Fulwiler CE, & Saper CB (1984). Subnuclear organization of the efferent connections of the parabrachial nucleus in the rat. Brain Res, 319(3), 229–259. [PubMed: 6478256]

Fulwiler CE, & Saper CB (1985). Cholecystokinin-immunoreactive innervation of the ventromedial hypothalamus in the rat: possible substrate for autonomic regulation of feeding. Neurosci Lett, 53(3), 289–296. 10.1016/0304-3940(85)90553-1 [PubMed: 3885078]

Garfield AS, Li C, Madara JC, Shah BP, Webber E, Steger JS, Campbell JN, Gavrilova O, Lee CE, Olson DP, Elmquist JK, Tannous BA, Krashes MJ, & Lowell BB (2015). A neural basis for melanocortin-4 receptor-regulated appetite. Nat Neurosci, 18(6), 863–871. 10.1038/nn.4011 [PubMed: 25915476]

Garfield AS, Shah BP, Madara JC, Burke LK, Patterson CM, Flak J, Neve RL, Evans ML, Lowell BB, Myers MG Jr., & Heisler LK (2014). A parabrachial-hypothalamic cholecystokinin neurocircuit controls counterregulatory responses to hypoglycemia. Cell Metab, 20(6), 1030–1037. 10.1016/j.cmet.2014.11.006 [PubMed: 25470549]

Gasparini S, Resch JM, Narayan SV, Peltekian L, Iverson GN, Karthik S, & Geerling JC (2019). Aldosterone-sensitive HSD2 neurons in mice. Brain Struct Funct, 224(1), 387–417. 10.1007/s00429-018-1778-y [PubMed: 30343334]

Geerling JC, Kim M, Mahoney CE, Abbott SB, Agostinelli LJ, Garfield AS, Krashes MJ, Lowell BB, & Scammell TE (2016). Genetic identity of thermosensory relay neurons in the lateral parabrachial nucleus. Am J Physiol Regul Integr Comp Physiol, 310(1), R41–54. 10.1152/ajpregu.00094.2015 [PubMed: 26491097]

Geerling JC, & Loewy AD (2007). Sodium deprivation and salt intake activate separate neuronal subpopulations in the nucleus of the solitary tract and the parabrachial complex. J Comp Neurol, 504(4), 379–403. 10.1002/cne.21452 [PubMed: 17663450]

Geerling JC, Stein MK, Miller RL, Shin JW, Gray PA, & Loewy AD (2011). FoxP2 expression defines dorsolateral pontine neurons activated by sodium deprivation. Brain Res, 1375, 19–27. 10.1016/j.brainres.2010.11.028 [PubMed: 21108936]

Geerling JC, Yokota S, Rukhadze I, Roe D, & Chamberlin NL (2017). Kolliker-Fuse GABAergic and glutamatergic neurons project to distinct targets. J Comp Neurol, 525(8), 1844–1860. 10.1002/cne.24164 [PubMed: 28032634]

Gent TC, Bandarabadi M, Herrera CG, & Adamantidis AR (2018). Thalamic dual control of sleep and wakefulness. Nat Neurosci, 21(7), 974–984. 10.1038/s41593-018-0164-7 [PubMed: 29892048]

Grady F, Peltekian L, Iverson G, & Geerling JC (2020). Direct Parabrachial-Cortical Connectivity. Cerebral Cortex.

Gray PA (2008). Transcription factors and the genetic organization of brain stem respiratory neurons. J Appl Physiol (1985), 104(5), 1513–1521. 10.1152/japplphysiol.01383.2007 [PubMed: 18218908]

Graybiel AM (1978). A satellite system of the superior colliculus: the parabigeminal nucleus and its projections to the superficial collicular layers. Brain Res, 145(2), 365–374. 10.1016/0006-8993(78)90870-3 [PubMed: 638795]

Guo CN, Machado NL, Zhan SQ, Yang XF, Yang WJ, & Lu J (2016). Identification of Cholinergic Pallidocortical Neurons. CNS Neurosci Ther, 22(10), 863–865. 10.1111/cns.12602 [PubMed: 27577268]

Han W, Tellez LA, Perkins MH, Perez IO, Qu T, Ferreira J, Ferreira TL, Quinn D, Liu ZW, Gao XB, Kaelberer MM, Bohorquez DV, Shammah-Lagnado SJ, de Lartigue G, & de Araujo IE (2018). A Neural Circuit for Gut-Induced Reward. Cell, 175(3), 887–888. 10.1016/j.cell.2018.10.018 [PubMed: 30340046]

Hayakawa T, Zheng JQ, & Seki M (1999). Direct parabrachial nuclear projections to the pharyngeal motoneurons in the rat: an anterograde and retrograde double-labeling study. Brain Res, 816(2), 364–374. 10.1016/s0006-8993(98)01127-5 [PubMed: 9878830]

Herbert H, Moga MM, & Saper CB (1990). Connections of the parabrachial nucleus with the nucleus of the solitary tract and the medullary reticular formation in the rat. J Comp Neurol, 293(4), 540–580. 10.1002/cne.902930404 [PubMed: 1691748]

Hermanson O, Larhammar D, & Blomqvist A (1998). Preprocholecystokinin mRNA-expressing neurons in the rat parabrachial nucleus: subnuclear localization, efferent projection, and expression of nociceptive-related intracellular signaling substances. J Comp Neurol, 400(2), 255–270. [PubMed: 9766403]

Hermanson O, Telkov M, Geijer T, Hallbeck M, & Blomqvist A (1998). Preprodynorphin mRNA-expressing neurones in the rat parabrachial nucleus: subnuclear localization, hypothalamic projections and colocalization with noxious-evoked fos-like immunoreactivity. Eur J Neurosci, 10(1), 358–367. 10.1046/j.1460-9568.1998.00021.x [PubMed: 9753144]

Hindman J, Bowren MD, Bruss J, Wright B, Geerling JC, & Boes AD (2018). Thalamic strokes that severely impair arousal extend into the brainstem. Ann Neurol, 84(6), 926–930. 10.1002/ana.25377 [PubMed: 30421457]

Hurley KM, Herbert H, Moga MM, & Saper CB (1991). Efferent projections of the infralimbic cortex of the rat. J Comp Neurol, 308(2), 249–276. 10.1002/cne.903080210 [PubMed: 1716270]

Jackson A, & Crossman AR (1983). Nucleus tegmenti pedunculopontinus: efferent connections with special reference to the basal ganglia, studied in the rat by anterograde and retrograde transport of horseradish peroxidase. Neuroscience, 10(3), 725–765. 10.1016/0306-4522(83)90213-0 [PubMed: 6646427]

Jarvie BC, & Palmiter RD (2017). HSD2 neurons in the hindbrain drive sodium appetite. Nat Neurosci, 20(2), 167–169. 10.1038/nn.4451 [PubMed: 27918529]

Jhou TC, Geisler S, Marinelli M, Degarmo BA, & Zahm DS (2009). The mesopontine rostromedial tegmental nucleus: A structure targeted by the lateral habenula that projects to the ventral tegmental area of Tsai and substantia nigra compacta. J Comp Neurol, 513(6), 566–596. 10.1002/cne.21891 [PubMed: 19235216]

Karimnamazi H, & Travers JB (1998). Differential projections from gustatory responsive regions of the parabrachial nucleus to the medulla and forebrain. Brain Res, 813(2), 283–302. 10.1016/s0006-8993(98)00951-2 [PubMed: 9838165]

Kaur S, Pedersen NP, Yokota S, Hur EE, Fuller PM, Lazarus M, Chamberlin NL, & Saper CB (2013). Glutamatergic signaling from the parabrachial nucleus plays a critical role in hypercapnic arousal. J Neurosci, 33(18), 7627–7640. 10.1523/JNEUROSCI.0173-13.2013 [PubMed: 23637157]

Kaur S, Wang JL, Ferrari L, Thankachan S, Kroeger D, Venner A, Lazarus M, Wellman A, Arrigoni E, Fuller PM, & Saper CB (2017). A Genetically Defined Circuit for Arousal from Sleep during Hypercapnia. Neuron, 96(5), 1153–1167 e1155. 10.1016/j.neuron.2017.10.009 [PubMed: 29103805]

Kim DY, Heo G, Kim M, Kinm H, Jin JA, Kim HK, Jung S, An M, Ahn BH, Park JH, Park HE, Lee H, Lee JW, Schwartz GJ, & Kim SY (2020). A neural circuit mechanism for mechanosensory feedback control of ingestion. Nature.

Krout KE, & Loewy AD (2000). Parabrachial nucleus projections to midline and intralaminar thalamic nuclei of the rat. J Comp Neurol, 428(3), 475–494. 10.1002/1096-9861(20001218)428:3<475::aid-cne6>3.0.co;2-9 [PubMed: 11074446]

Krukoff TL, Harris KH, & Jhamandas JH (1993). Efferent projections from the parabrachial nucleus demonstrated with the anterograde tracer Phaseolus vulgaris leucoagglutinin. Brain Res Bull, 30(1–2), 163–172. 10.1016/0361-9230(93)90054-f [PubMed: 7678381]

Kudo M, & Niimi K (1978). Ascending projections of the inferior colliculus onto the medial geniculate body in the cat studied by anterograde and retrograde tracing techniques. Brain Res, 155(1), 113–117. 10.1016/0006-8993(78)90310-4 [PubMed: 688004]

Ledoux JE, Ruggiero DA, Forest R, Stornetta R, & Reis DJ (1987). Topographic organization of convergent projections to the thalamus from the inferior colliculus and spinal cord in the rat. J Comp Neurol, 264(1), 123–146. 10.1002/cne.902640110 [PubMed: 2445791]

Lee H, Kim DW, Remedios R, Anthony TE, Chang A, Madisen L, Zeng H, & Anderson DJ (2014). Scalable control of mounting and attack by Esr1+ neurons in the ventromedial hypothalamus. Nature, 509(7502), 627–632. 10.1038/nature13169 [PubMed: 24739975]

Lee S, Augustine V, Zhao Y, Ebisu H, Ho B, Kong D, & Oka Y (2019). Chemosensory modulation of neural circuits for sodium appetite. Nature, 568(7750), 93–97. 10.1038/s41586-019-1053-2 [PubMed: 30918407]

Li MM, Madara JC, Steger JS, Krashes MJ, Balthasar N, Campbell JN, Resch JM, Conley NJ, Garfield AS, & Lowell BB (2019). The Paraventricular Hypothalamus Regulates Satiety and Prevents Obesity via Two Genetically Distinct Circuits. Neuron, 102(3), 653–667 e656. 10.1016/j.neuron.2019.02.028 [PubMed: 30879785]

Lin D, Boyle MP, Dollar P, Lee H, Lein ES, Perona P, & Anderson DJ (2011). Functional identification of an aggression locus in the mouse hypothalamus. Nature, 470(7333), 221–226. 10.1038/nature09736 [PubMed: 21307935]

Miller RL, Knuepfer MM, Wang MH, Denny GO, Gray PA, & Loewy AD (2012). Fos-activation of FoxP2 and Lmx1b neurons in the parabrachial nucleus evoked by hypotension and hypertension in conscious rats. Neuroscience, 218, 110–125. 10.1016/j.neuroscience.2012.05.049 [PubMed: 22641087]

Moga MM, Herbert H, Hurley KM, Yasui Y, Gray TS, & Saper CB (1990). Organization of cortical, basal forebrain, and hypothalamic afferents to the parabrachial nucleus in the rat. J Comp Neurol, 295(4), 624–661. 10.1002/cne.902950408 [PubMed: 1694187]

Mu D, Deng J, Liu KF, Wu ZY, Shi YF, Guo WM, Mao QQ, Liu XJ, Li H, & Sun YG (2017). A central neural circuit for itch sensation. Science, 357(6352), 695–699. 10.1126/science.aaf4918 [PubMed: 28818946]

Nakamura K, & Morrison SF (2008). A thermosensory pathway that controls body temperature. Nature neuroscience, 11(1), 62–71. 10.1038/nn2027 [PubMed: 18084288]

Nakamura K, & Morrison SF (2010). A thermosensory pathway mediating heat-defense responses. Proc Natl Acad Sci U S A, 107(19), 8848–8853. 10.1073/pnas.0913358107 [PubMed: 20421477]

Niu JG, Yokota S, Tsumori T, Qin Y, & Yasui Y (2010). Glutamatergic lateral parabrachial neurons innervate orexin-containing hypothalamic neurons in the rat. Brain Res, 1358, 110–122. 10.1016/j.brainres.2010.08.056 [PubMed: 20735997]

Norgren R (1976). Taste pathways to hypothalamus and amygdala. J Comp Neurol, 166(1), 17–30. 10.1002/cne.901660103 [PubMed: 1262547]

Norgren R, & Leonard CM (1971). Taste pathways in rat brainstem. Science, 173(4002), 1136–1139. [PubMed: 4329178]

Norgren R, & Leonard CM (1973). Ascending central gustatory pathways. J Comp Neurol, 150(2), 217–237. 10.1002/cne.901500208 [PubMed: 4723066]

Palmiter RD (2018). The Parabrachial Nucleus: CGRP Neurons Function as a General Alarm. Trends Neurosci, 41(5), 280–293. 10.1016/j.tins.2018.03.007 [PubMed: 29703377]

Park S, Williams KW, Liu C, & Sohn JW (2020). A neural basis for tonic suppression of sodium appetite. Nat Neurosci. 10.1038/s41593-019-0573-2

Paxinos G, & Franklin KBJ (2013). Paxinos and Franklin's The mouse brain in stereotaxic coordinates (Fourth edition. ed.). Academic Press, an imprint of Elsevier.

Paxinos G, & Watson C (2007). The rat brain in stereotaxic coordinates (6th ed.). Academic Press/Elsevier.

Perrotti LI, Bolanos CA, Choi KH, Russo SJ, Edwards S, Ulery PG, Wallace DL, Self DW, Nestler EJ, & Barrot M (2005). DeltaFosB accumulates in a GABAergic cell population in the posterior tail of the ventral tegmental area after psychostimulant treatment. Eur J Neurosci, 21(10), 2817–2824. 10.1111/j.1460-9568.2005.04110.x [PubMed: 15926929]

Petreanu L, Huber D, Sobczyk A, & Svoboda K (2007). Channelrhodopsin-2-assisted circuit mapping of long-range callosal projections. Nat Neurosci, 10(5), 663–668. 10.1038/nn1891 [PubMed: 17435752]

Price JL, & Stern R (1983). Individual cells in the nucleus basalis--diagonal band complex have restricted axonal projections to the cerebral cortex in the rat. Brain Res, 269(2), 352–356. 10.1016/0006-8993(83)90145-2 [PubMed: 6883087]

Qiu MH, Chen MC, Fuller PM, & Lu J (2016). Stimulation of the Pontine Parabrachial Nucleus Promotes Wakefulness via Extra-thalamic Forebrain Circuit Nodes. Curr Biol, 26(17), 2301–2312. 10.1016/j.cub.2016.07.054 [PubMed: 27546576]

Ren S, Wang Y, Yue F, Cheng X, Dang R, Qiao Q, Sun X, Li X, Jiang Q, Yao J, Qin H, Wang G, Liao X, Gao D, Xia J, Zhang J, Hu B, Yan J, Wang Y, Xu M, Han Y, Tang X, Chen X, He C, & Hu Z (2018). The paraventricular thalamus is a critical thalamic area for wakefulness. Science, 362(6413), 429–434. 10.1126/science.aat2512 [PubMed: 30361367]

Resch JM, Fenselau H, Madara JC, Wu C, Campbell JN, Lyubetskaya A, Dawes BA, Tsai LT, Li MM, Livneh Y, Ke Q, Kang PM, Fejes-Toth G, Naray-Fejes-Toth A, Geerling JC, & Lowell BB (2017). Aldosterone-Sensing Neurons in the NTS Exhibit State-Dependent Pacemaker Activity and Drive Sodium Appetite via Synergy with Angiotensin II Signaling. Neuron, 96(1), 190–206 e197. 10.1016/j.neuron.2017.09.014 [PubMed: 28957668]

Rose MF, Ahmad KA, Thaller C, & Zoghbi HY (2009). Excitatory neurons of the proprioceptive, interoceptive, and arousal hindbrain networks share a developmental requirement for Math1. Proc Natl Acad Sci U S A, 106(52), 22462–22467. 10.1073/pnas.0911579106 [PubMed: 20080794]

Ruigrok TJ (2003). Collateralization of climbing and mossy fibers projecting to the nodulus and flocculus of the rat cerebellum. J Comp Neurol, 466(2), 278–298. 10.1002/cne.10889 [PubMed: 14528453]

Ryan PJ, Ross SI, Campos CA, Derkach VA, & Palmiter RD (2017). Oxytocin-receptor-expressing neurons in the parabrachial nucleus regulate fluid intake. Nat Neurosci, 20(12), 1722–1733. 10.1038/s41593-017-0014-z [PubMed: 29184212]

Santiago AC, & Shammah-Lagnado SJ (2005). Afferent connections of the amygdalopiriform transition area in the rat. J Comp Neurol, 489(3), 349–371. 10.1002/cne.20637 [PubMed: 16025448]

Saper CB (1982). Reciprocal parabrachial-cortical connections in the rat. Brain Res, 242(1), 33–40. [PubMed: 7104731]

Saper CB (2016). The House Alarm. Cell Metab, 23(5), 754–755. 10.1016/j.cmet.2016.04.021 [PubMed: 27166934]

Saper CB, & Loewy AD (1980). Efferent connections of the parabrachial nucleus in the rat. Brain Res, 197(2), 291–317. [PubMed: 7407557]

Saunders A, Oldenburg IA, Berezovskii VK, Johnson CA, Kingery ND, Elliott HL, Xie T, Gerfen CR, & Sabatini BL (2015). A direct GABAergic output from the basal ganglia to frontal cortex. Nature, 521(7550), 85–89. 10.1038/nature14179 [PubMed: 25739505]

Sawchenko PE, & Swanson LW (1982). The organization of noradrenergic pathways from the brainstem to the paraventricular and supraoptic nuclei in the rat. Brain Res, 257(3), 275–325. 10.1016/0165-0173(82)90010-8 [PubMed: 6756545]

Shin JW, Geerling JC, Stein MK, Miller RL, & Loewy AD (2011). FoxP2 brainstem neurons project to sodium appetite regulatory sites. J Chem Neuroanat, 42(1), 1–23. 10.1016/j.jchemneu.2011.05.003 [PubMed: 21605659]

St John WM, Glasser RL, & King RA (1972). Rhythmic respiration in awake vagotomized cats with chronic pneumotaxic area lesions. Respir Physiol, 15(2), 233–244. [PubMed: 5042169]

Stornetta RL, Sevigny CP, & Guyenet PG (2002). Vesicular glutamate transporter DNPI/VGLUT2 mRNA is present in C1 and several other groups of brainstem catecholaminergic neurons. J Comp Neurol, 444(3), 191–206. 10.1002/cne.10141 [PubMed: 11840474]

Swanson LW (1992). Brain maps : structure of the rat brain. Elsevier.

Taylor AM, Jeffery G, & Lieberman AR (1986). Subcortical afferent and efferent connections of the superior colliculus in the rat and comparisons between albino and pigmented strains. Exp Brain Res, 62(1), 131–142. 10.1007/bf00237409 [PubMed: 3956628]

Thompson RH, & Swanson LW (1998). Organization of inputs to the dorsomedial nucleus of the hypothalamus: a reexamination with Fluorogold and PHAL in the rat. Brain Res Brain Res Rev, 27(2), 89–118. 10.1016/s0165-0173(98)00010-1 [PubMed: 9622601]

Tokita K, Inoue T, & Boughter JD Jr. (2009). Afferent connections of the parabrachial nucleus in C57BL/6J mice. Neuroscience, 161(2), 475–488. 10.1016/j.neuroscience.2009.03.046 [PubMed: 19327389]

Tokita K, Inoue T, & Boughter JD Jr. (2010). Subnuclear organization of parabrachial efferents to the thalamus, amygdala and lateral hypothalamus in C57BL/6J mice: a quantitative retrograde double labeling study. Neuroscience, 171(1), 351–365. 10.1016/j.neuroscience.2010.08.026 [PubMed: 20832453]

Travers JB, & Norgren R (1983). Afferent projections to the oral motor nuclei in the rat. J Comp Neurol, 220(3), 280–298. 10.1002/cne.902200303 [PubMed: 6315785]

Ungerstedt U (1971). Stereotaxic mapping of the monoamine pathways in the rat brain. Acta Physiol Scand Suppl, 367, 1–48. 10.1111/j.1365-201x.1971.tb10998.x [PubMed: 4109331]

Van der Werf YD, Witter MP, & Groenewegen HJ (2002). The intralaminar and midline nuclei of the thalamus. Anatomical and functional evidence for participation in processes of arousal and awareness. Brain Res Brain Res Rev, 39(2–3), 107–140. 10.1016/s0165-0173(02)00181-9 [PubMed: 12423763]

Verstegen AMJ, Vanderhorst V, Gray PA, Zeidel ML, & Geerling JC (2017a). Barrington's nucleus: Neuroanatomic landscape of the mouse "pontine micturition center". J Comp Neurol, 525(10), 2287–2309. 10.1002/cne.24215 [PubMed: 28340519]

Verstegen AMJ, Vanderhorst V, Gray PA, Zeidel ML, & Geerling JC (2017b). Barrington's nucleus: Neuroanatomic landscape of the mouse "pontine micturition center". J Comp Neurol. 10.1002/cne.24215

Wang VY, Rose MF, & Zoghbi HY (2005). Math1 expression redefines the rhombic lip derivatives and reveals novel lineages within the brainstem and cerebellum. Neuron, 48(1), 31–43. 10.1016/j.neuron.2005.08.024 [PubMed: 16202707]

Wiedenmann B, & Franke WW (1985). Identification and localization of synaptophysin, an integral membrane glycoprotein of Mr 38,000 characteristic of presynaptic vesicles. Cell, 41(3), 1017–1028. 10.1016/s0092-8674(85)80082-9 [PubMed: 3924408]

Wouterlood FG, & Jorritsma-Byham B (1993). The anterograde neuroanatomical tracer biotinylated dextran-amine: comparison with the tracer Phaseolus vulgaris-leucoagglutinin in preparations for electron microscopy. J Neurosci Methods, 48(1–2), 75–87. 10.1016/s0165-0270(05)80009-3 [PubMed: 7690870]

Wu Q, Clark MS, & Palmiter RD (2012). Deciphering a neuronal circuit that mediates appetite. Nature, 483(7391), 594–597. 10.1038/nature10899 [PubMed: 22419158]

Yahiro T, Kataoka N, Nakamura Y, & Nakamura K (2017). The lateral parabrachial nucleus, but not the thalamus, mediates thermosensory pathways for behavioural thermoregulation. Sci Rep, 7(1), 5031 10.1038/s41598-017-05327-8 [PubMed: 28694517]

Yang CF, Chiang MC, Gray DC, Prabhakaran M, Alvarado M, Juntti SA, Unger EK, Wells JA, & Shah NM (2013). Sexually dimorphic neurons in the ventromedial hypothalamus govern mating in both sexes and aggression in males. Cell, 153(4), 896–909. 10.1016/j.cell.2013.04.017 [PubMed: 23663785]

Yasui Y, Saper CB, & Cechetto DF (1989). Calcitonin gene-related peptide immunoreactivity in the visceral sensory cortex, thalamus, and related pathways in the rat. J Comp Neurol, 290(4), 487–501. 10.1002/cne.902900404 [PubMed: 2613940]

Yokota S, Kaur S, VanderHorst VG, Saper CB, & Chamberlin NL (2015). Respiratory-related outputs of glutamatergic, hypercapnia-responsive parabrachial neurons in mice. J Comp Neurol, 523(6), 907–920. 10.1002/cne.23720 [PubMed: 25424719]

Yoshida A, Chen K, Moritani M, Yabuta NH, Nagase Y, Takemura M, & Shigenaga Y (1997). Organization of the descending projections from the parabrachial nucleus to the trigeminal sensory nuclear complex and spinal dorsal horn in the rat. J Comp Neurol, 383(1), 94–111. [PubMed: 9184989]

Zaborszky L, Beinfeld MC, Palkovits M, & Heimer L (1984). Brainstem projection to the hypothalamic ventromedial nucleus in the rat: a CCK-containing long ascending pathway. Brain Res, 303(2), 225–231. 10.1016/0006-8993(84)91208-3 [PubMed: 6611191]

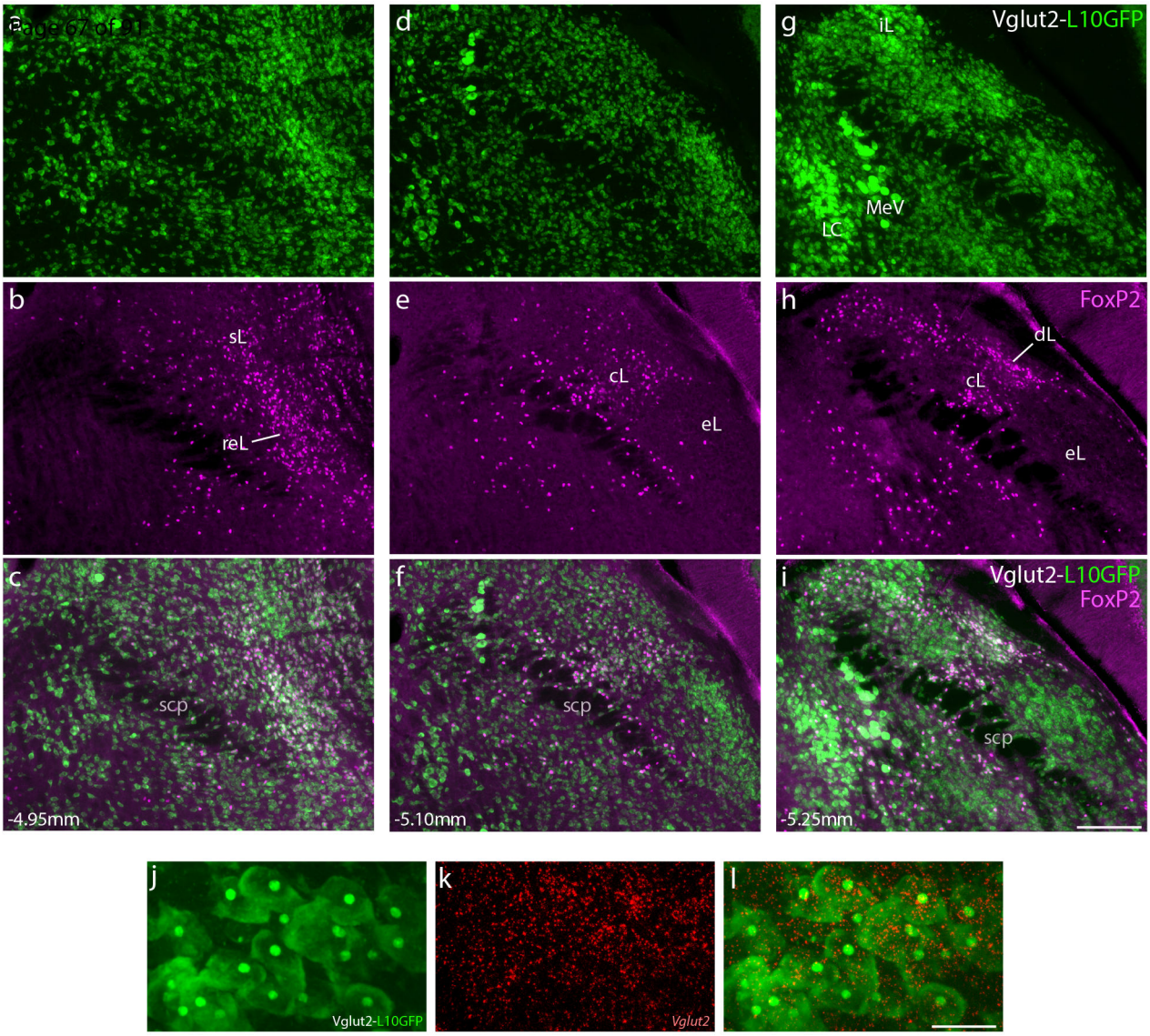

Figure 1.

Neurons that express the transcription factor FoxP2 form a subset of the larger population of glutamatergic neurons in the parabrachial nucleus (PB). (a–i) Across three levels of the PB region, Cre-reporter expression reveals the distribution of neurons that have expressed vesicular glutamate transporter 2 (Vglut2). Approximate bregma level is shown at the bottom-left of each column. Green fluorescent protein (conjugated to the L10 ribosomal subunit; L10GFP) in *Vglut2-IRES-Cre;R26-lsl-L10GFP* mice represents neurons that have expressed Vglut2. Note that this includes neurons in the locus coeruleus (LC), which no longer express Vglut2 in the adult brain (Stornetta et al., 2002). Neurons with nuclear immunofluorescence labeling for FoxP2 (magenta) span the dorsal lateral (dL), central lateral (cL), rostral to external lateral (reL), and superior lateral (sL) PB subnuclei. In contrast, FoxP2 labeling is sparse in the external lateral (eL) subnucleus. Scale bar in (i) is 200 μm and applies to panels (a-i). (j-l) GFP-expressing neurons in the lateral PB neurons contain mRNA for Vglut2 (*Slc17a6*). Scale bar in (l) is 20 μm and applies to panels (j-k).

Other abbreviations: iL, internal lateral; MeV, mesencephalic trigeminal nucleus; scp, superior cerebellar peduncle.

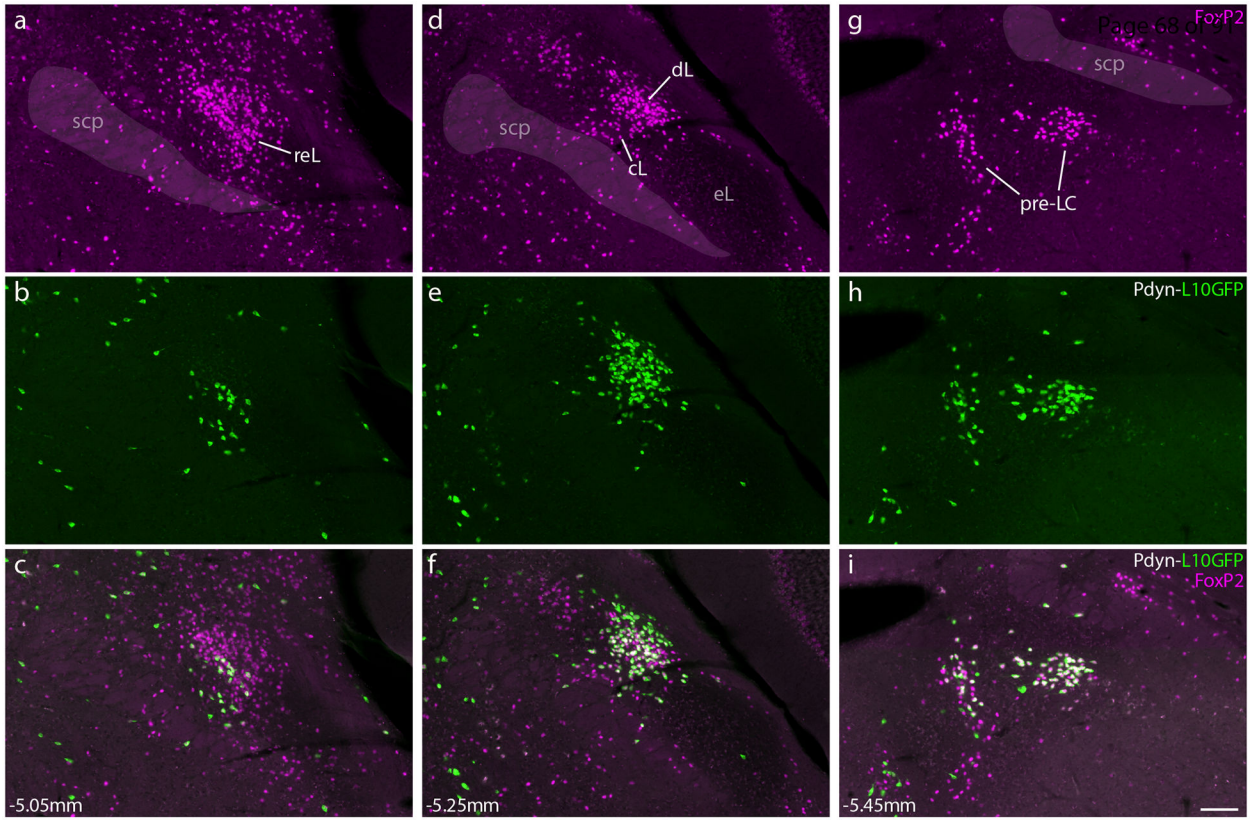

Figure 2.

Neurons that express the neuropeptide gene *Pdyn* form a subset of the larger FoxP2 population in the PB. (a, d, g) Immunofluorescence labeling for FoxP2 (magenta) at three rostrocaudal levels of the PB, from (a) PBreL, back through (d) PBdL and PBcL, and caudally to (g) the pre-LC. (b, e, h) Green fluorescent protein (conjugated to the L10 ribosomal subunit; L10GFP) in *Pdyn-IRES-Cre;R26-lsl-L10GFP* mice represents neurons that have expressed *Pdyn*. (c, f, i) Merged images show the co-localization of FoxP2-immunoreactive nuclei with L10GFP reporter. Approximate bregma level show at bottom-left. Scale bar is 100 μm and applies to all panels.

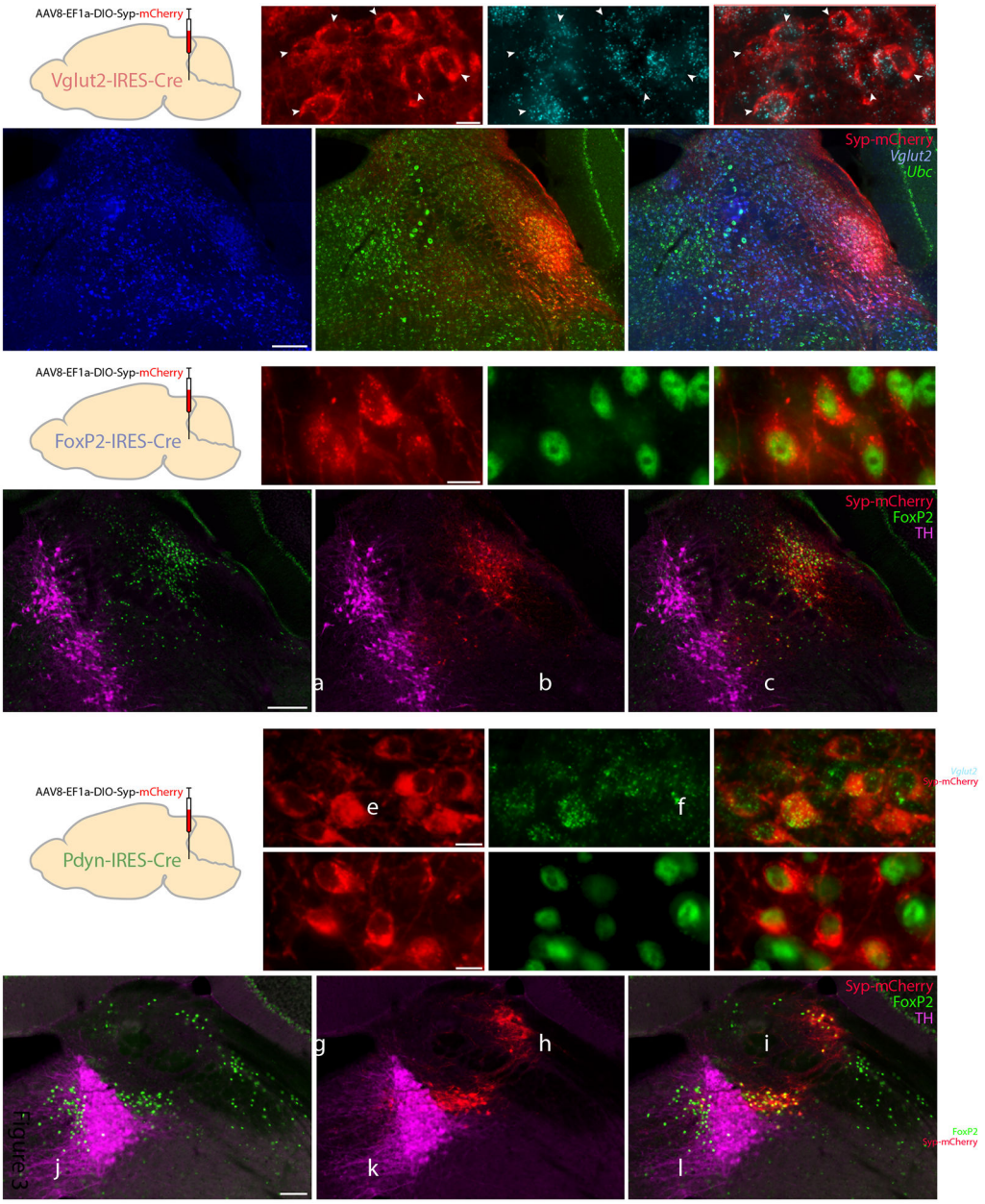

Figure 3.

Cre-conditional expression of synaptophysin(Syp)-mCherry in each Cre-driver strain. (a–f): Syp-mCherry (red) expression in a *Vglut2-IRES-Cre* mouse (case 1281), along with *in situ* hybridization for *Slc17a6* (Vglut2, blue) and *Ubc* (ubiquitin c, green). White arrowheads indicate Syp-mCherry-expressing PB neurons with mRNA labeling for *Slc17a6*. Scale bar in (a) is 10 μm and applies to (b–c). Scale bar in (d) is 200 μm and applies to (e–f). (g–l): Syp-mCherry expression in a *FoxP2-IRES-Cre* mouse (case 1405), with immunofluorescence labeling for FoxP2 (green) and tyrosine hydroxylase (TH, magenta). Scale bar in (g) is 10 μm and applies to (h–i). Scale bar in (j) is 200 μm and applies to (k–l). (m–o): Syp-mCherry (red) expression in a *Pdyn-IRES-Cre* mouse (case #1814), with fluorescence *in situ* hybridization for *Pdyn* mRNA (green). (p–u): Syp-mCherry expression in a *Pdyn-IRES-Cre*

mouse (case 1812), with immunofluorescence labeling for FoxP2 (green) and TH (magenta). Scale bars in (m) and (p) are 10 μm and apply to (n–o) and (q–r), respectively. Scale bar in (s) is 100 μm and applies to (t–u).

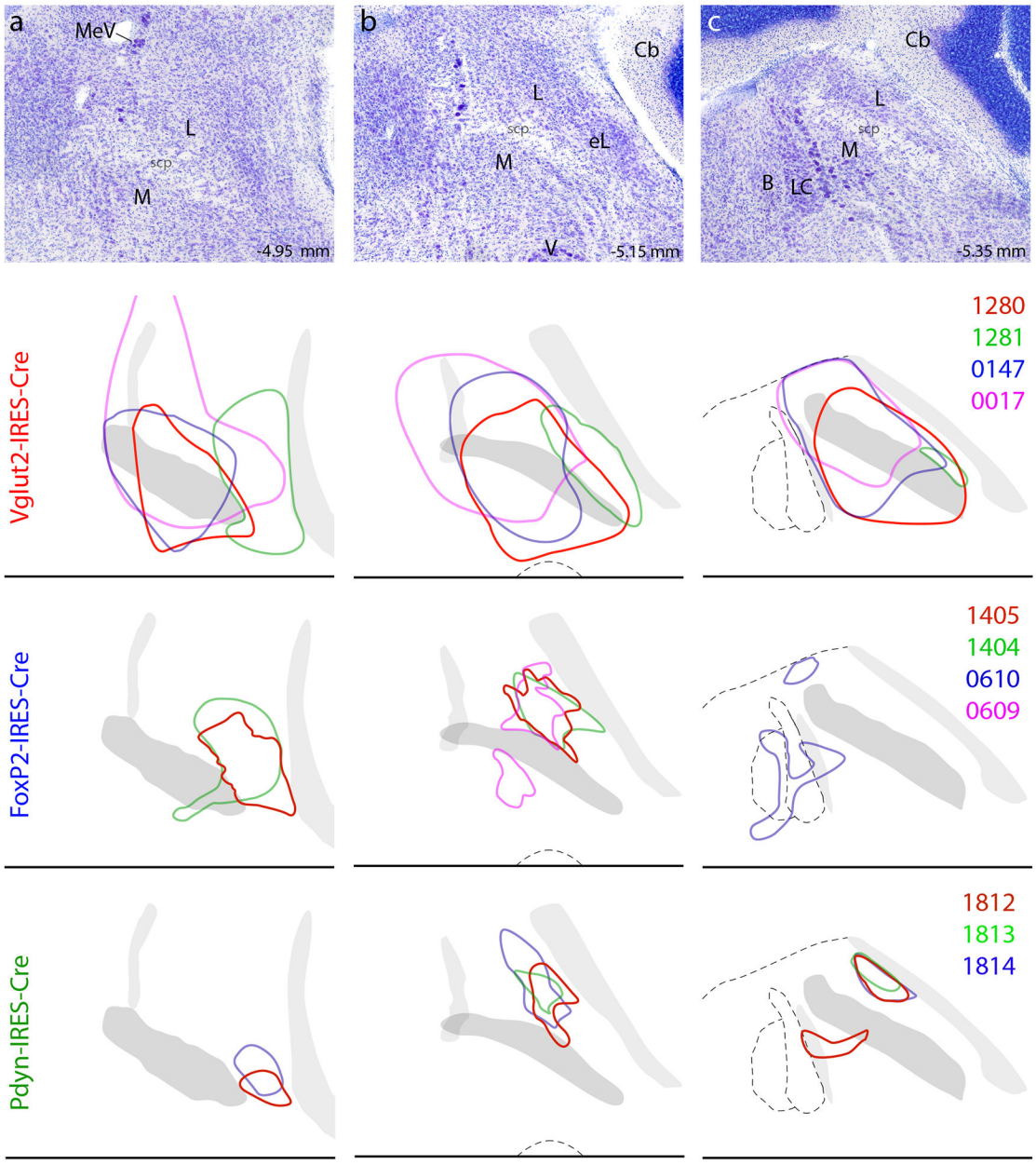

Figure 4.

Location and distribution of Syp-mCherry-transduced neurons in each case. The top row (a–c) shows Nissl cytoarchitecture at three rostrocaudal levels of the PB region, with approximate bregma levels at bottom-right. Color outlines show the location of the core cluster of Syp-mCherry-transduced neurons in that case (case numbers at right), separated by Cre-driver strain. Other abbreviations: B, Barrington's nucleus; Cb, cerebellum; L, lateral PB subdivision; M, medial PB subdivision; V, motor nucleus of the trigeminal (Vth cranial) nerve.

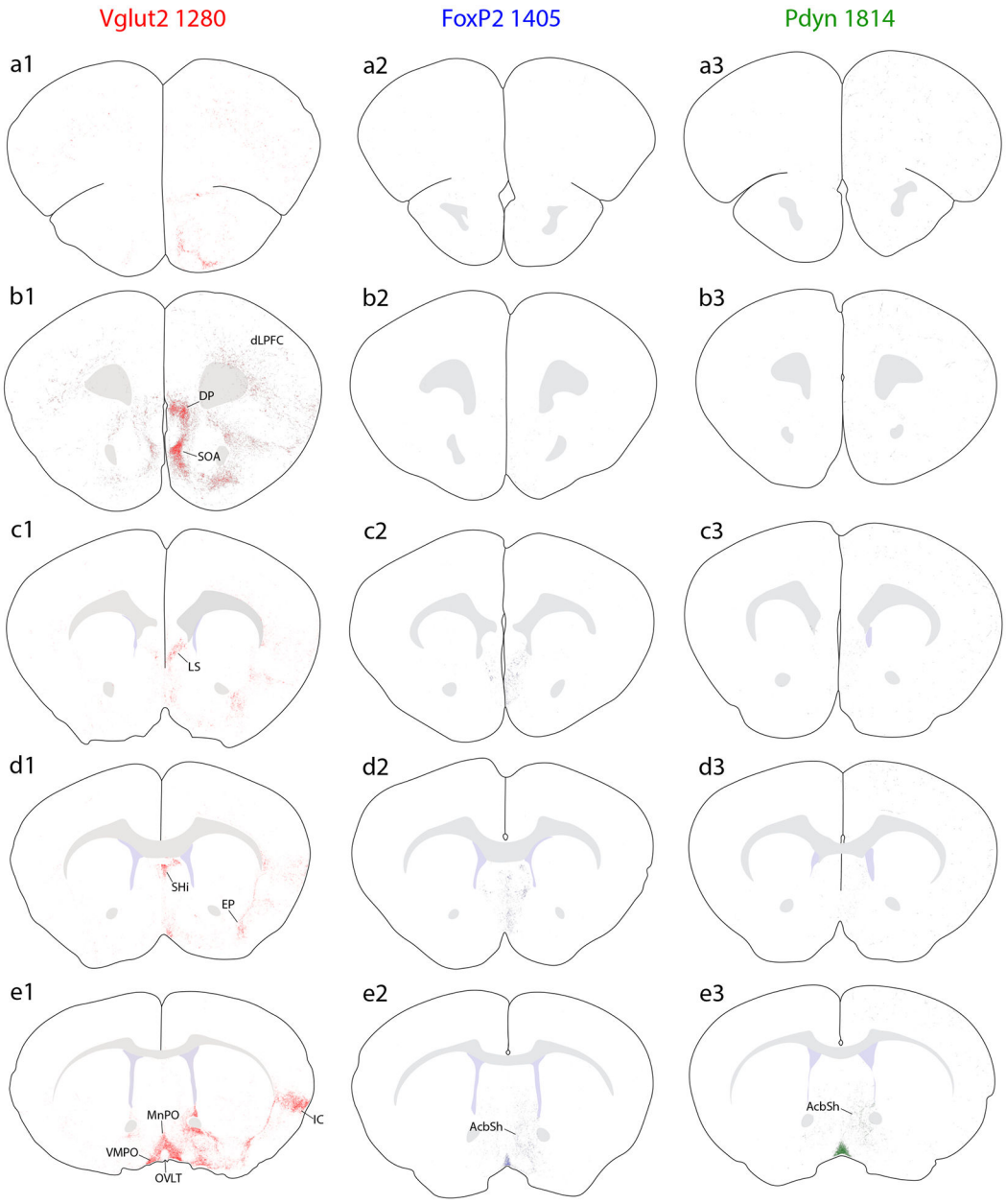

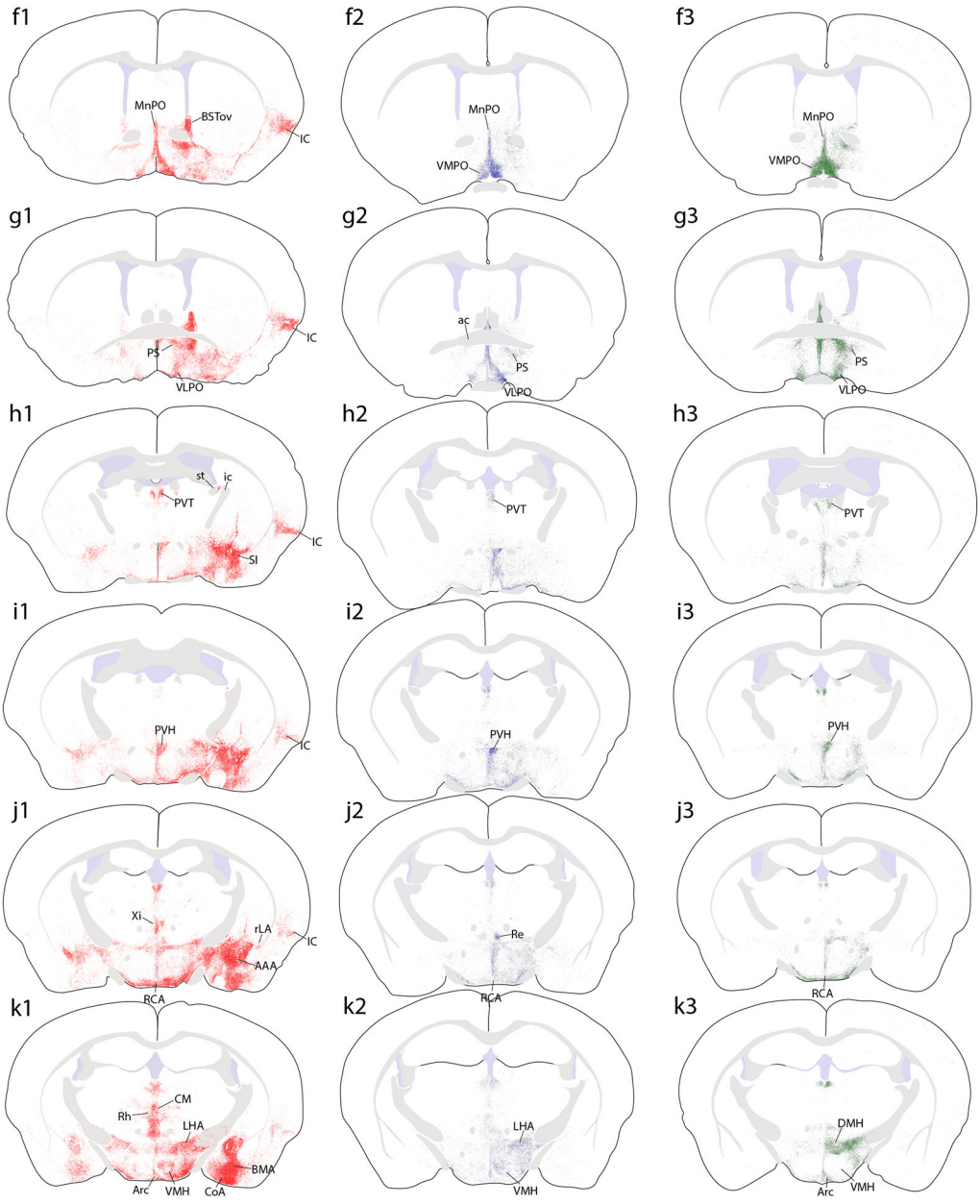

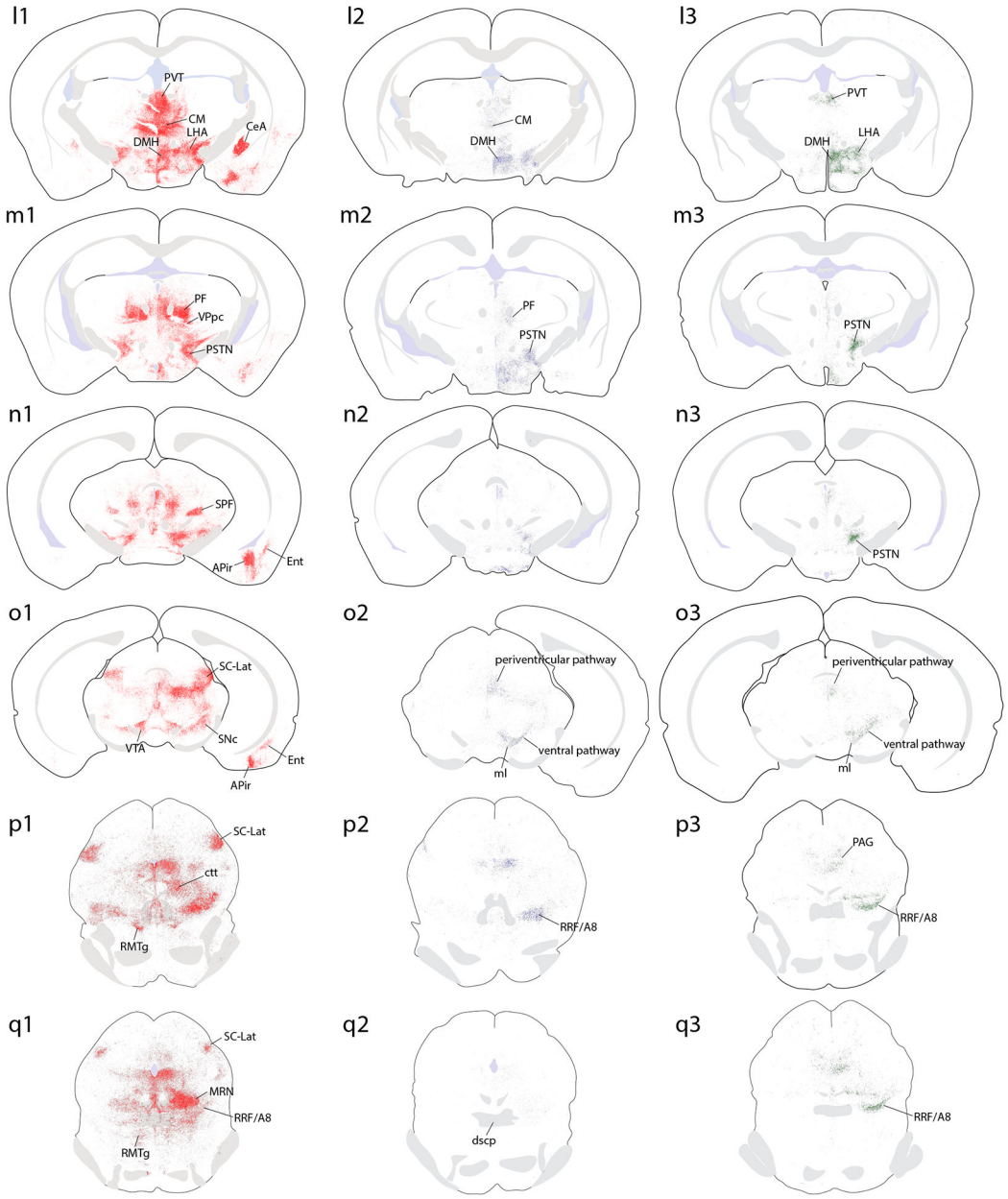

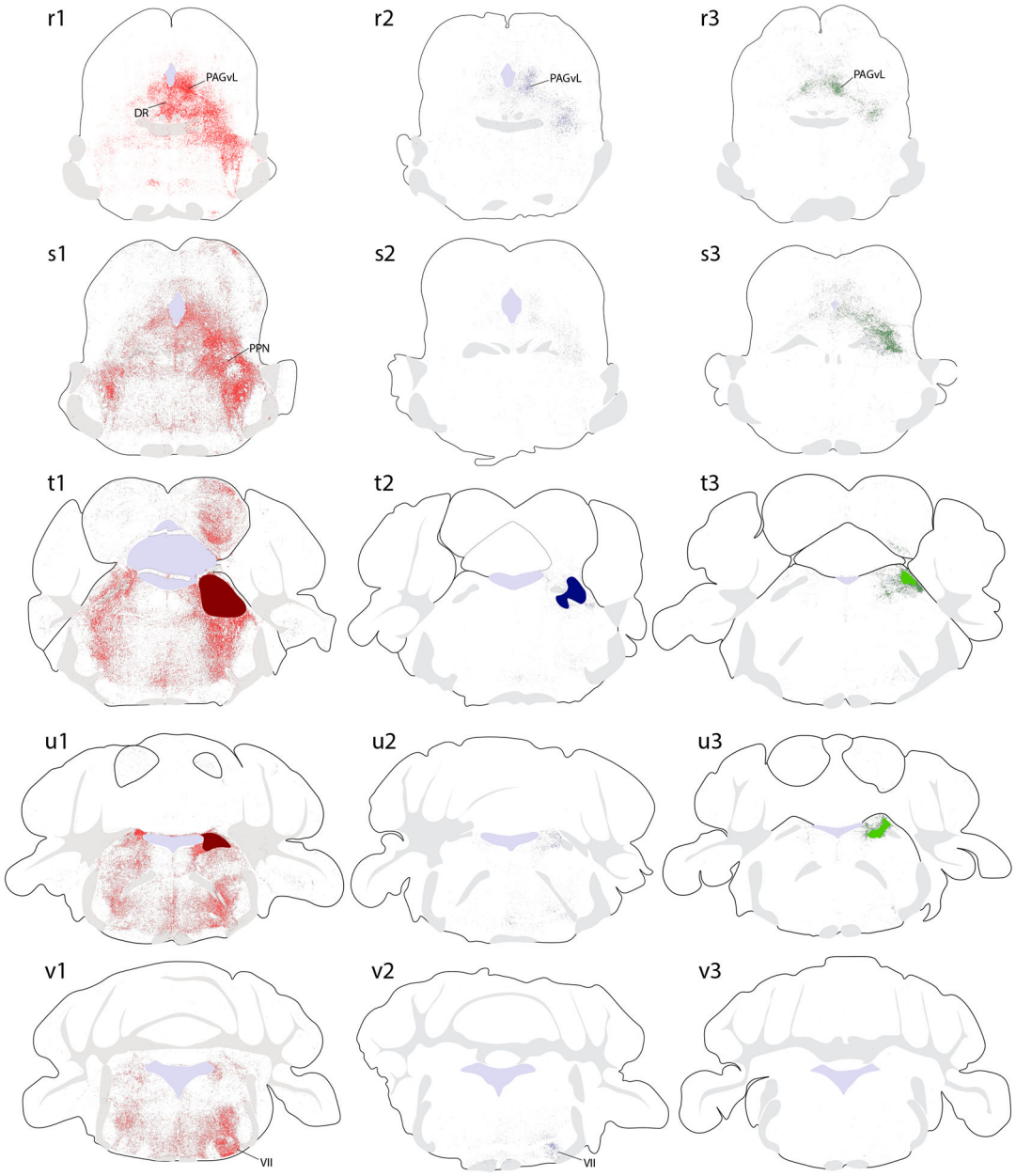

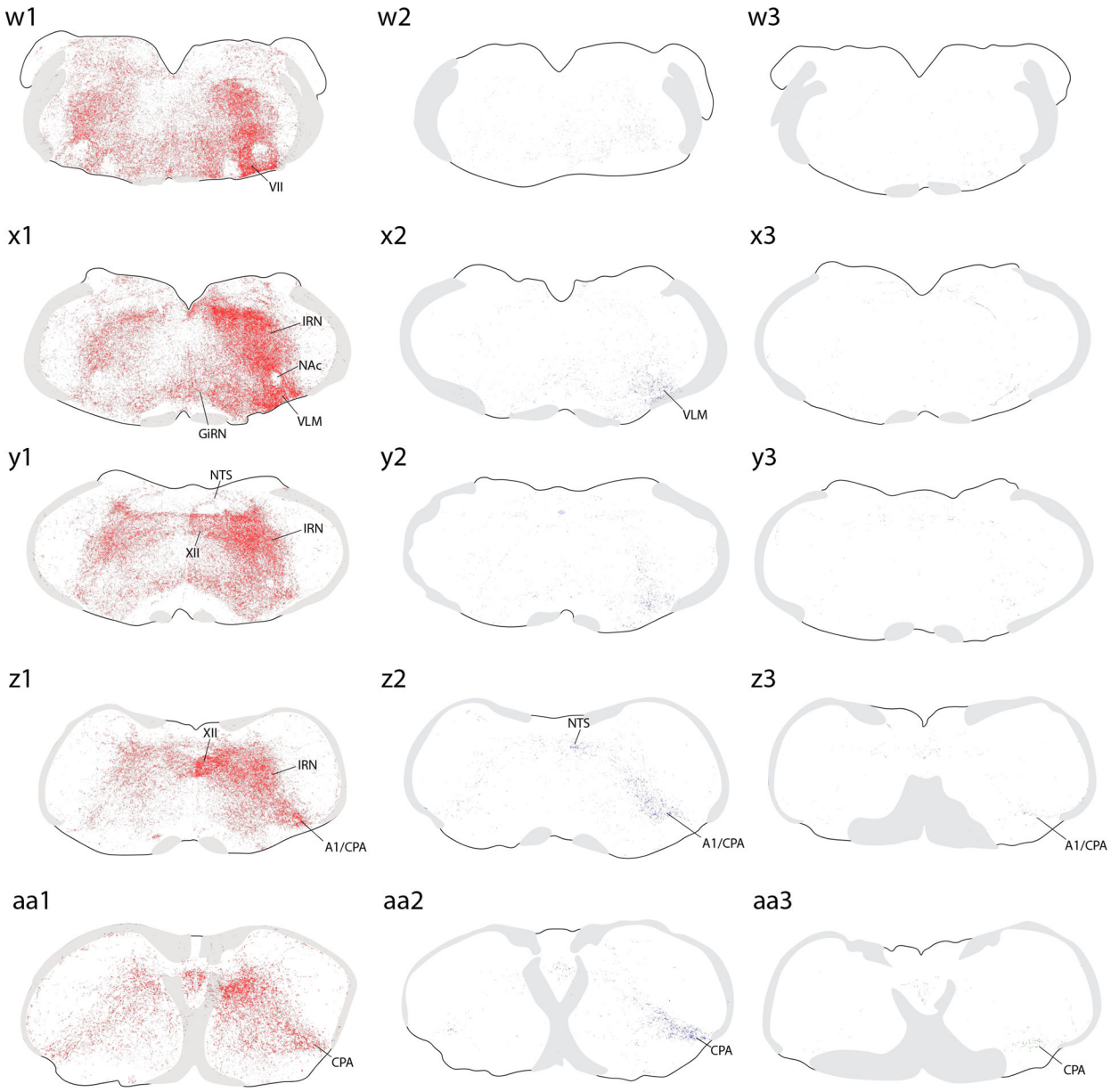

Figure 5.

Brain-wide plots of punctate immunolabeling for Syp-mCherry, representing putative presynaptic boutons of virally transduced neurons in the PB region. Representative cases from each Cre-driver strain are shown in separate colors in each column (*Vglut2-IRES-Cre* case 1280, red; *FoxP2-IRES-Cre* case 1405, blue; *Pdyn-IRES-Cre* case 1814, green). The 27 illustrated sections in each row (a–aa) were chosen to match the rostrocaudal level and section angle between cases as closely as possible. The solid color in panels (s1–3) represents the region of heavy somatic and dendritic immunolabeling at the core of each injection site. Other abbreviations: see **List of Abbreviations**.

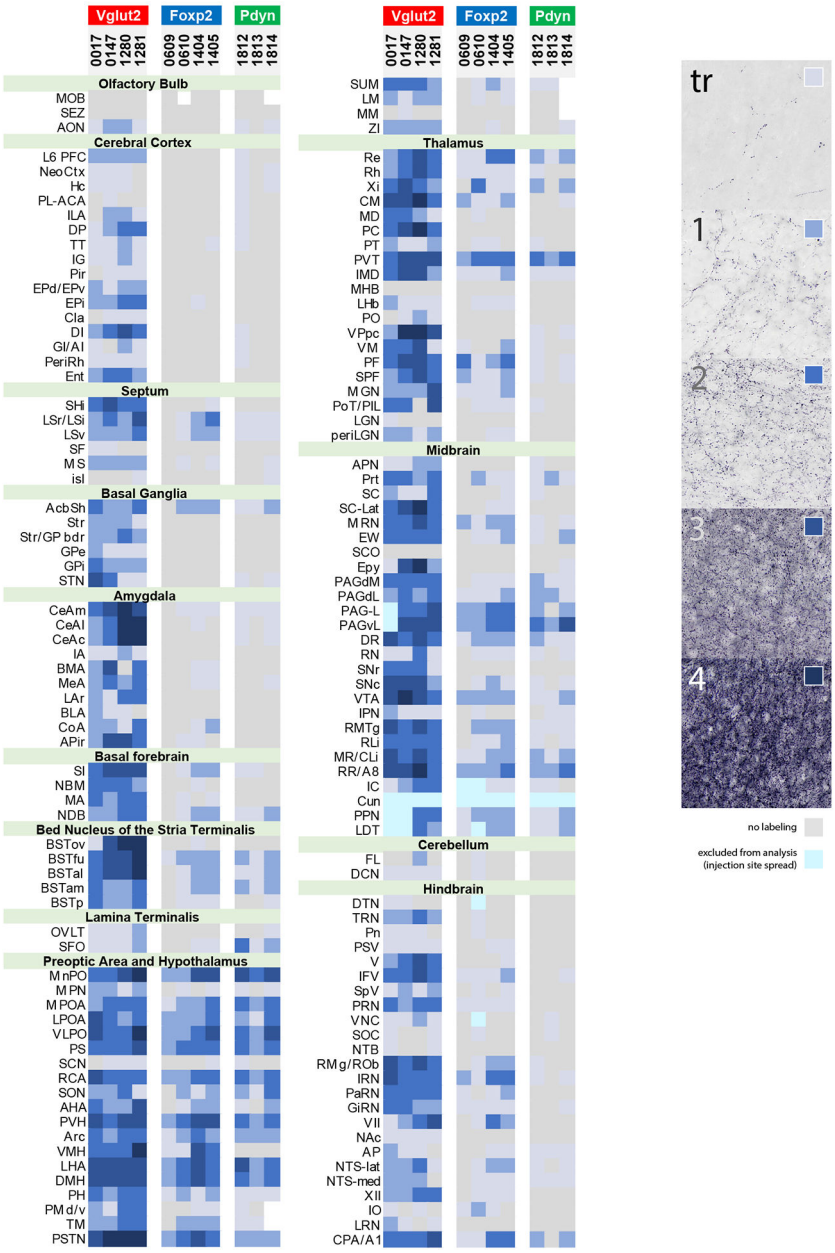

Figure 6.

Density of Syp-mCherry-labeled punctae across 147 brain regions in each PB-injected case, grouped by Cre-driver strain. The density standards we used to rate each region are shown at right. Gray indicates an absence of Syp-mCherry labeling. Light-to-dark shades of blue represent increasing densities of punctae. Ice-blue represents regions that were excluded from analysis due to Syp-mCherry labeling in cell bodies and/or dendrites near the injection site. White represents areas that could not be analyzed due to histologic artifacts. Abbreviation: tr, trace labeling.

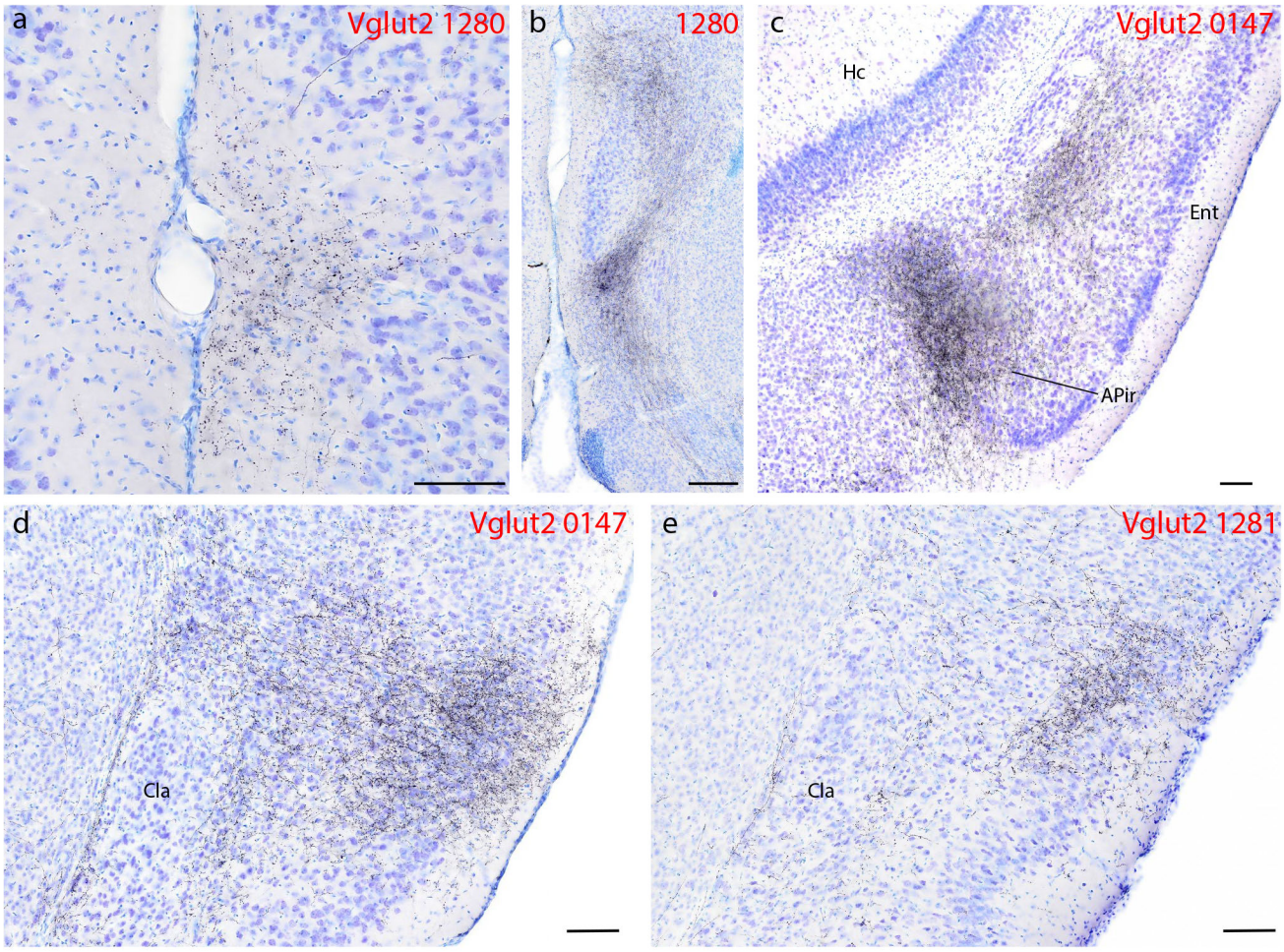

Figure 7.

Syp-mCherry labeling (black, NiDAB) in the cerebral cortex of Vglut2 cases (case numbers at upper-right of each panel). (a) Moderately dense labeling in the medial prefrontal cortex, within the thicker molecular layer (layer 1) of the dorsal peduncular cortex immediately ventral to the infralimbic area (Hurley et al., 1991). (b) Dense labeling in the "septo-olfactory area" aggregates dorsal and ventral to the tenia tecta, which has a thickened layer 2 (Hurley et al., 1991). (c) Dense Syp-mCherry labeling in layer 5 of the rostral entorhinal (Ent) cortex and in the amygdalopiriform transition cortex (APir). (d) Dense glutamatergic Syp-mCherry labeling covers all layers of the mid-insular cortex, but avoids the principal claustrum nucleus (CLA). In one Vglut2 case with an injection site centered in the lateral PB (1281), labeling in the insular cortex clustered superficially, over layer 3. All scale bars are 100 μm. Other abbreviations: Hc, hippocampus.

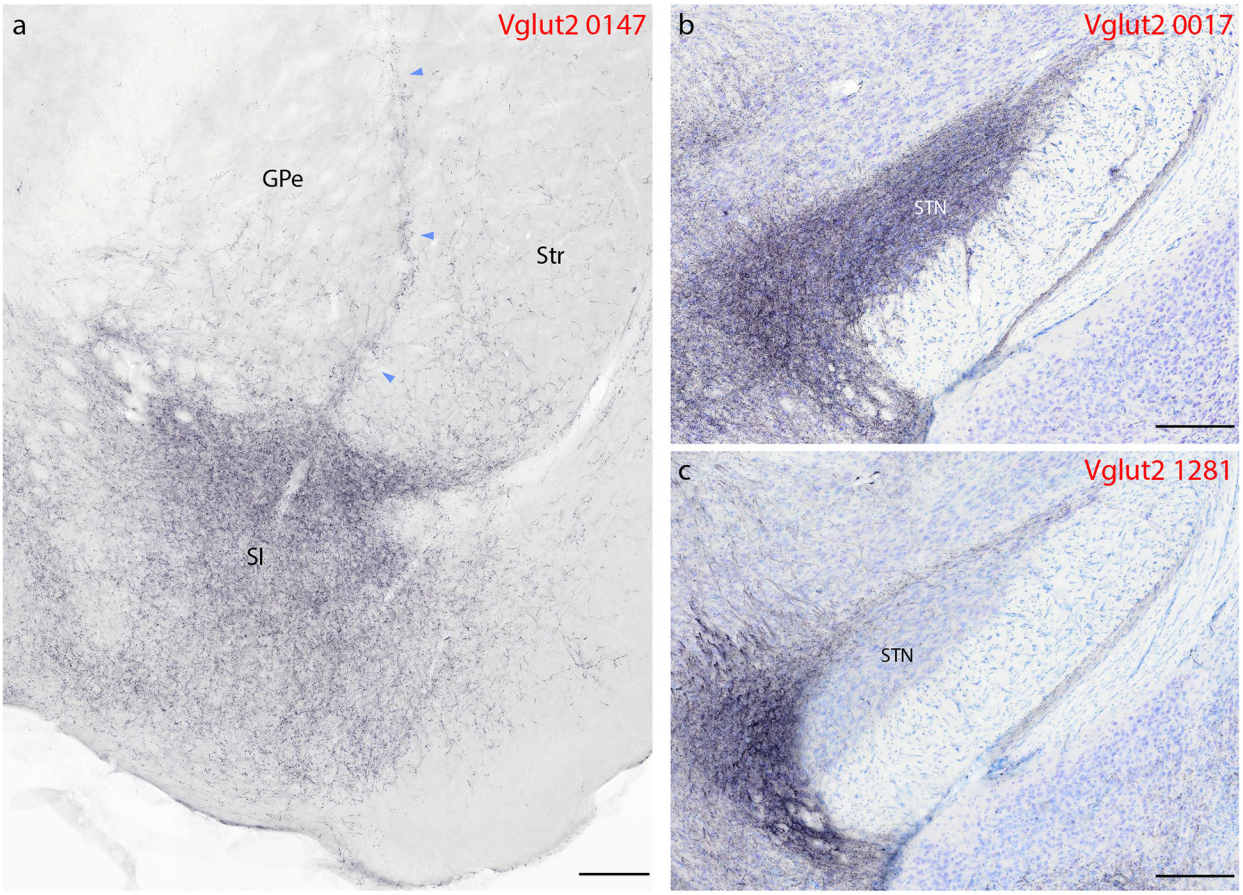

Figure 8.

Syp-mCherry labeling in basal forebrain and basal ganglia. (a) In addition to light punctate labeling in both the striatum (Str) and globus pallidus (GPe), a band of Syp-mCherry-labeled boutons extends dorsally between these two structures, up from a dense terminal field in the basal forebrain, primarily within the substantia innominata (SI). (b–c) We found dense labeling in the subthalamic nucleus (STN) in only one case, where the injection site spread rostrally from the PB into the pedunculopontine tegmental area (b, 0017). Vglut2 case 1281 (c) and other Vglut2 cases had little to no labeling in the STN. Other abbreviations: ic, internal capsule; ot, optic tract. Scale bars are 200 μm.

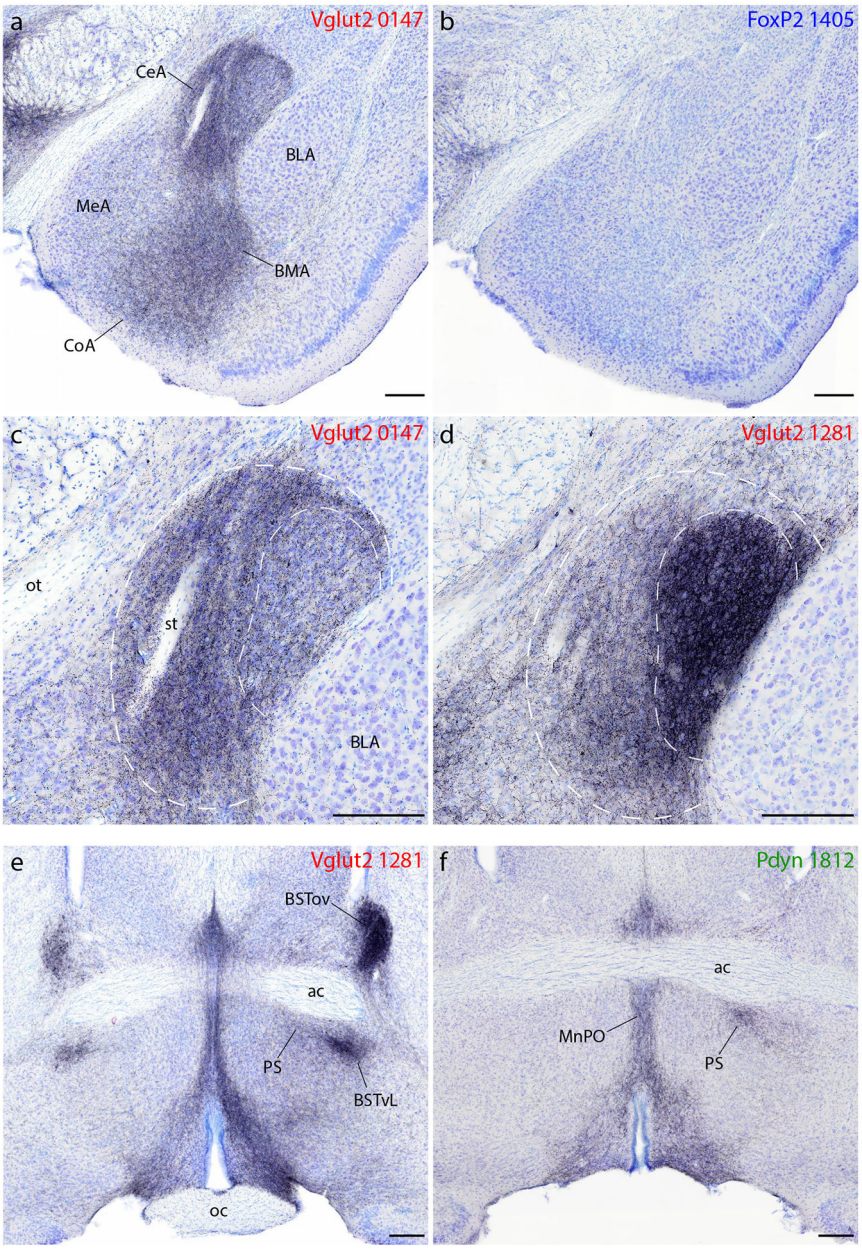

Figure 9.

Syp-mCherry labeling in the amygdala, bed nucleus of the stria terminalis (BST), and preoptic area. (a–b) All Vglut2 cases had dense labeling in the central (CeA), basomedial (BMA), and cortical (CoA) nuclei of the amygdala and lighter labeling in the medial nucleus (MeA), with little to no labeling in the basolateral nucleus (BLA). (b) FoxP2 (and Pdyn) cases had virtually no Syp-mCherry labeling in the amygdala. (c–d) Injection site location within the PB affects the distribution of labeling within the CeA. An injection site centered in the medial PB (c, case 0147) produced denser Syp-mCherry labeling in the medial CeA subdivision (outer dashed line), while an injection into the lateral PB (d, case 1281) produced denser labeling in the combined lateral and lateral capsular CeA subdivisions (inner dashed line). (e–f) Vglut2 cases contained dense labeling in the anterior, lateral BST.

In this region of the BST, the densest labeling in the oval subnucleus (BSTov) appeared after an injection centered in PBeL (e, case 1281). Vglut2 cases also had consistently heavy labeling in a focal subregion of the ventrolateral BST (BSTvL) and in the adjoining preoptic parastrial nucleus (PS), as well as the median preoptic nucleus (MnPO). (f) Pdyn (and FoxP2) cases had much lighter labeling in the BST, but similarly dense Syp-mCherry labeling in the PS and MnPO. Other abbreviations: ac, anterior commissure; oc, optic chiasm; st, stria terminalis. Scale bars are all 200 μm.

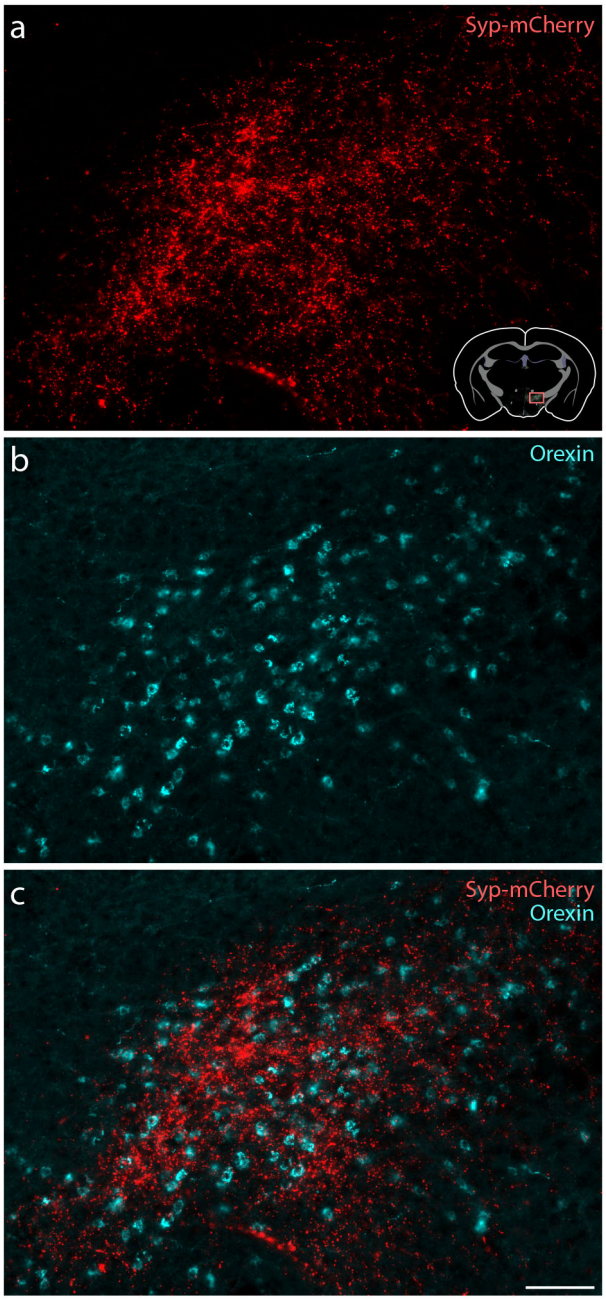

Figure 10.

In the LHA of Pdyn cases, the distribution of Syp-mCherry-labeled boutons (a,c; red) had a striking overlap with the distribution of neurons that are immunoreactive for the neuropeptide orexin (also known as hypocretin; ice-blue in b–c). Scale bar is 100 μm.

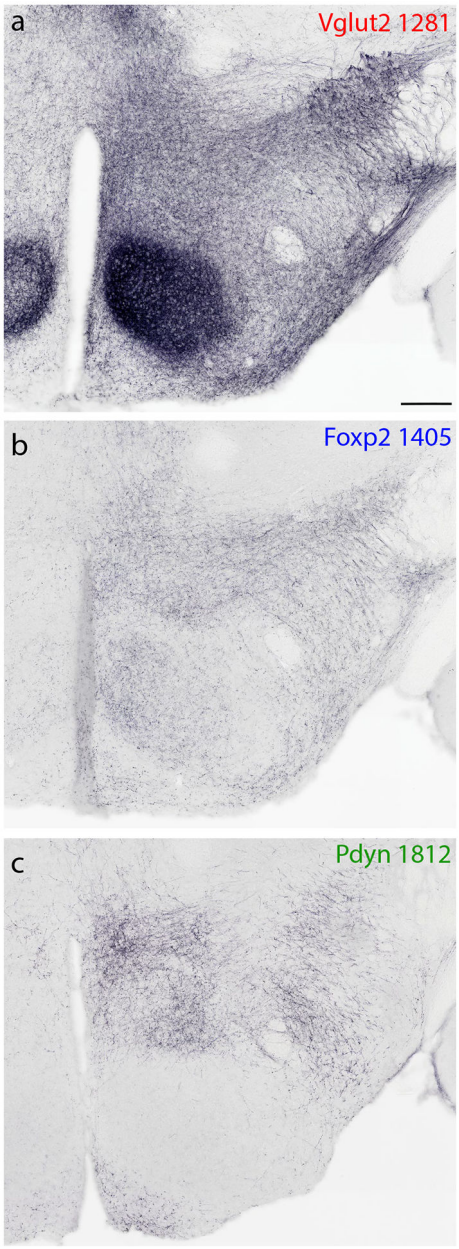

Figure 11.

Syp-mCherry labeling at a middle (tuberal) level of the hypothalamus, showing the prominent differences in labeling density within the ventromedial hypothalamic nucleus (VMH). (a) Vglut2 cases had variable labeling densities in the VMH, with by far the densest arising after an injection into the lateral PB (case 1281). (b) FoxP2 cases had lighter labeling in the VMH, while (c) Pdyn cases had virtually none. All cases had prominent labeling in the hypothalamic dorsomedial, lateral, and arcuate nuclei. Scale bar is 200 μm.

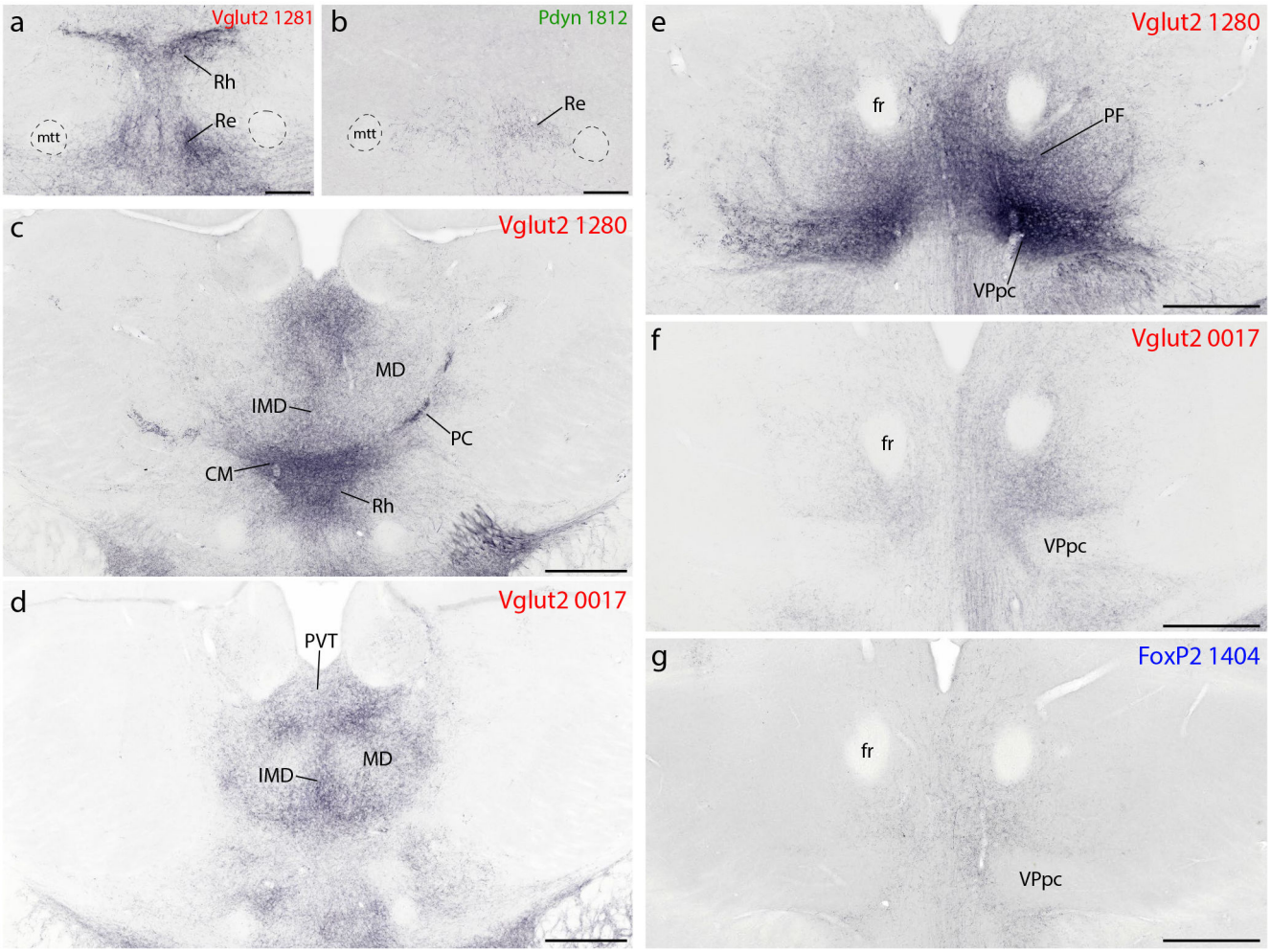

Figure 12.

Syp-mCherry labeling in the thalamus. (a–b) The reuniens (Re) thalamic nucleus contained labeling in all cases. This labeling was densest in Vglut2 cases, accompanied by similarly dense labeling in the overlying rhomboid (Rh) nucleus. (c–d) Across Vglut2 cases, projections from the PB region to the midline and intralaminar thalamic nuclei was varied and somewhat complementary. For example, injections centered in the medial PB subdivision (Vglut2 case 1280, a) produced heavy labeling in the centromedian (CM) and paracentral (PC) thalamic nuclei, with lighter labeling in the mediodorsal (MD) thalamic nuclei and moderately dense labeling in the midline intermediodorsal (IMD) nucleus. In contrast, an injection located rostrally and dorsally in the PB region (Vglut2 case 0017) left CM and PC almost devoid of labeling, despite similarly dense labeling in MD and IMD, and produced additional labeling rostrally, in the centrolateral (CL) intralaminar nucleus (not shown). All cases had moderately dense labeling throughout the paraventricular thalamic nucleus (PVT). Caudal levels of the thalamus (e–f) also received distinctly different projection patterns from the PB region. Specifically, (e) most Vglut2 cases had dense Syp-mCherry labeling in the parafasciular (PF) thalamic nucleus, surrounding the fasciculus retroflexus (fr), and immediately ventral to it in the parvicellular subdivision of the ventroposterior thalamic nucleus (VPpc). In contrast, (f) case 0017 had no labeling in the

VPpc and modest labeling in the PF. (g) FoxP2 cases had even lighter labeling in the PF, and none in VPpc. Scale bars are 200 μm in (a–b) and 500 μm in (c–g).

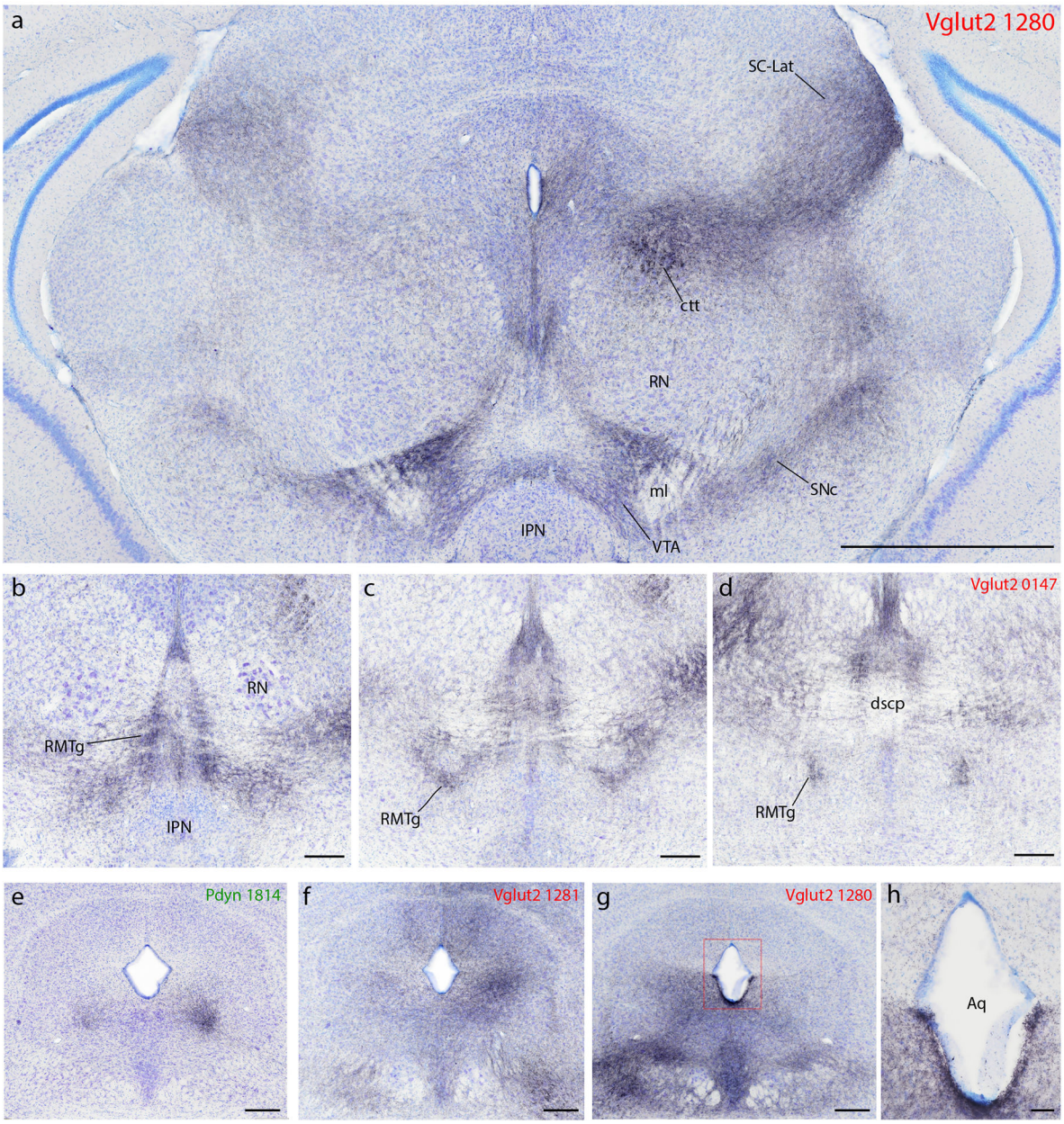

Figure 13.

Syp-mCherry labeling in the midbrain. (a) Dorsally, all Vglut2 cases had labeling in axons coursing through the central tegmental tract (ctt) and producing a terminal field through the midbrain reticular formation, which extended into the lateral, deep layers of the superior colliculus (SC-Lat). A parallel pathway and terminal field pervaded all levels of the periaqueductal gray matter (PAG). Ventrally, all Vglut2 cases had a moderately dense terminal field in the ventral tegmental area (VTA). This was the only brainstem region with similar or denser labeling on the contralateral side. Labeling here surrounds the medial lemniscus (ml) and arcs over the interpeduncular nucleus (IPN). This VTA terminal field was continuous with a dense terminal field laterally, in the substantia nigra pars compacta (SNc), which was continuous with dense labeling in the A8/retrorubral field caudally. The

red nucleus (RN), which contained little or no labeling, separated the dorsal and ventral terminal fields in the midbrain, with a lateral band of Syp-mCherry-labeled punctae running between it and the medial geniculate nucleus. (b–c) Extending caudally and dorsally from the VTA, all Vglut2 cases had a moderately dense terminal field in a region described as the “tail of the VTA” or rostromedial tegmental area (RMTg), which runs between the IPN/VTA rostro-ventrally, and the decussation of the scp (dscp) caudo-dorsally. (e–g) The PAG received a variety of different input projections, including a more focal input to its (e) ventrolateral column in Pdyn cases or a broader Vglut2 projection to its (g) lateral plus ventrolateral or in some cases (f) dorsal subdivisions. Also in this region, (h) we observed dense Syp-mCherry labeling throughout the ventral ependyma of the ventral cerebral aqueduct, exclusively in Vglut2 cases.

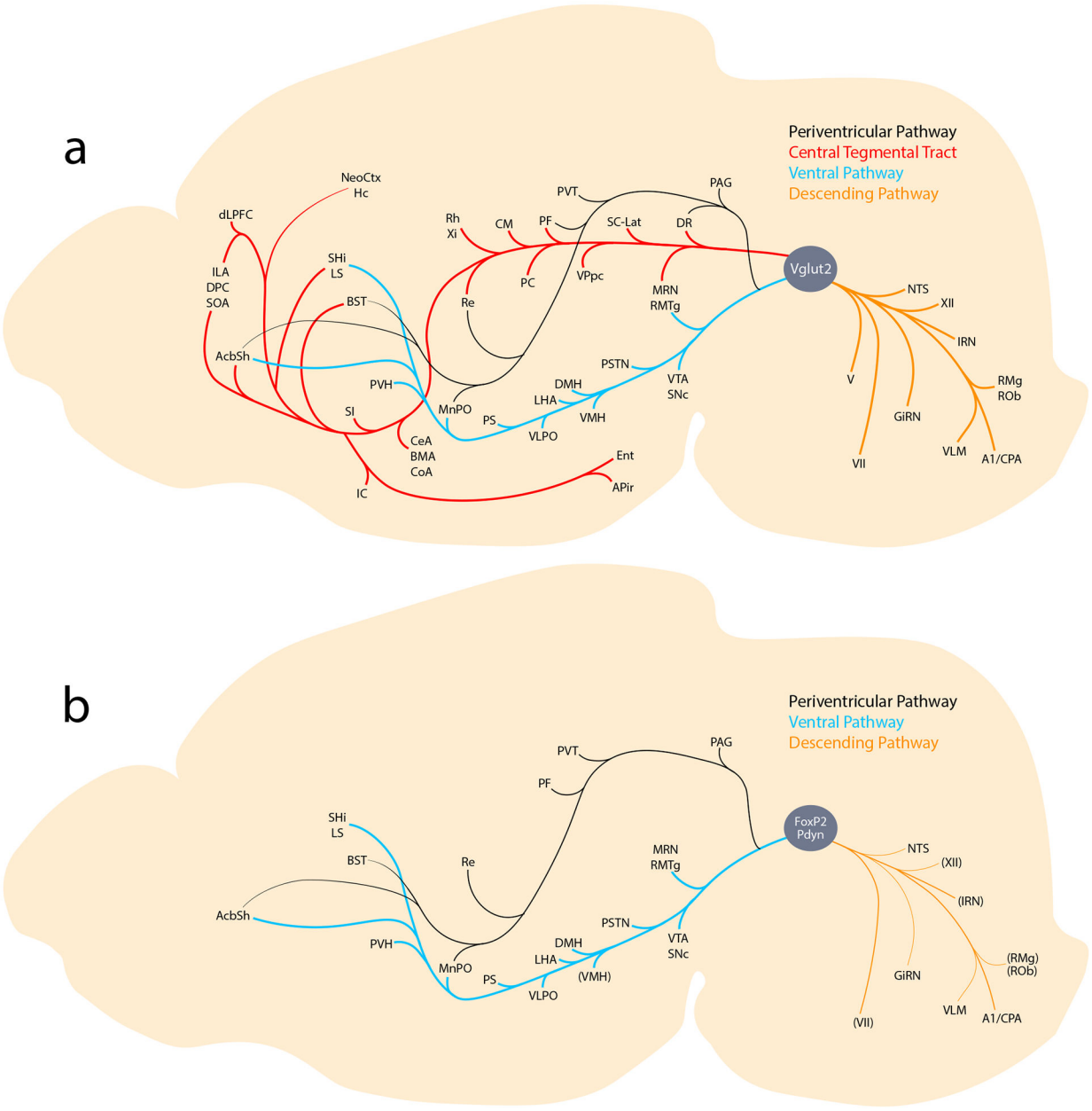

Figure 14.

Axonal pathways and efferent target sites of (a) Vglut2 and (b) FoxP2 and Pdyn neurons in the PB region. In (b), note that the VMH and several hindbrain nuclei (in parentheses) receive input from *Foxp2*-expressing neurons, but do not appear to receive any input from *Pdyn*-expressing neurons in the PB region.

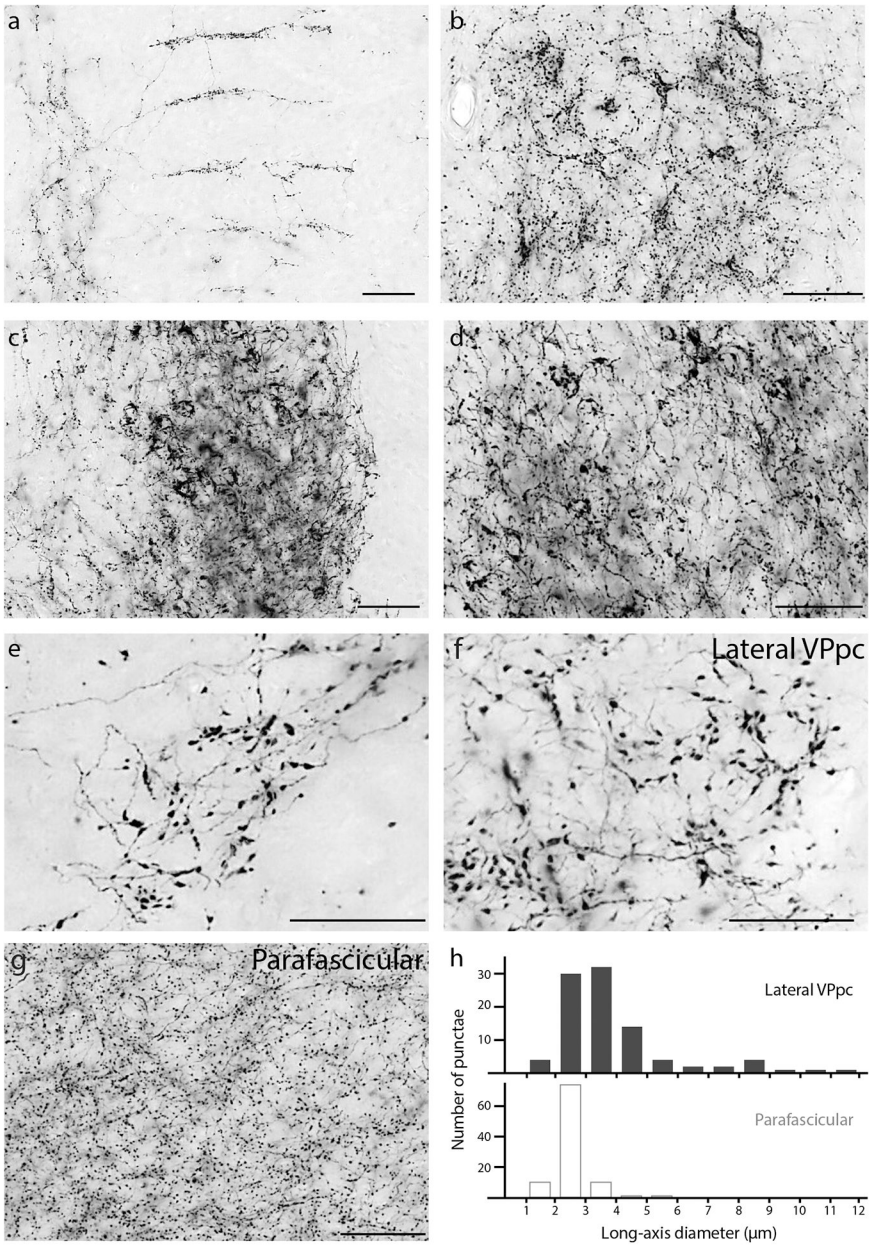

Figure 15.

Atypical morphologies of Syp-mCherry-labeled boutons in the: (a) Medial prefrontal cortex (infralimbic area; right side is medial); (b) Septohippocampal nucleus; (c) Oval BST subnucleus; (d) Lateral capsular subdivision of the CeA; (e) PC thalamic nucleus; (f) VPpc (lateral) thalamic nucleus; and (g) PF thalamic nucleus. The large boutons in the PC and lateral VPpc (e–f) form a striking contrast with the uniformly small, grainy appearance of boutons in the neighboring PF (g), which is the typical appearance of PB terminal fields in most other brain regions. (h) The distribution of bouton sizes (long-axis diameter) in the lateral VPpc includes many with larger diameters than in the dorsally adjacent PF.

Table 1.

Cre driver and reporter mice used in this study

Strain	Reference	Source information	Key gene
Vglut2-IRES-Cre (Slc17a6-IRES-Cre)	Vong, Linh, et al. "Leptin action on GABAergic neurons prevents obesity and reduces inhibitory tone to POMC neurons." *Neuron* 71.1 (2011): 142–154.	Jax 016963 https://www.jax.org/strain/016963	IRES-Cre inserted downstream of the stop codon of *Slc17a6* on chromosome 7
Foxp2-IRES-Cre	Rousso, David L., et al. "Two pairs of ON and OFF retinal ganglion cells are defined by intersectional patterns of transcription factor expression." *Cell reports* 15.9 (2016): 1930–1944.	Richard Palmiter lab, University of Washington Jax 030541 https://www.jax.org/strain/030541	IRES-Cre inserted after termination codon of the mouse *Foxp2* gene
Pdyn-IRES-Cre	Krashes, Michael J., et al. "An excitatory paraventricular nucleus to AgRP neuron circuit that drives hunger." *Nature* 507.7491 (2014): 238.	Jax 027958 https://www.jax.org/strain/027958	IRES-Cre inserted downstream of the endogenous Pdyn (prodynorphin) gene
R26-LSL-L10GFP reporter	Krashes, Michael J., et al. "An excitatory paraventricular nucleus to AgRP neuron circuit that drives hunger." *Nature* 507.7491 (2014): 238.	Available from originating investigators http://www.informatics.jax.org/allele/MGI:5559562	Floxed transcription STOP cassette followed by EGFP/Rpl10 fusion reporter gene under control of the CAG promoter targeted to the Gt(ROSA)26Sor locus

Table 2.

Antisera used in this study

Antigen	Immunogen description	Source, Host Species, RRID	Concentration
DsRed	DsRed-Express, a variant of *Discosoma sp.* red fluorescent protein	Clontech, rabbit polyclonal, cat. # 632496, lot# 1509043, RRID: AB_1001313483.	1:2,000
mCherry	Full length mCherry fluorescent protein	Life Sciences, rat monoclonal, cat.# M11217, lot# R1240561, RRID: AB_2536611	1:2,000
Forkhead box protein 2 (FoxP2)	Recombinant human FOXP2 isoform 1 Ala640-Glu715	R&D Systems, sheep polyclonal, cat.# AF5647, RRID: AB_2107133	1:10,000
Orexin / hypocretin	Full-length (33 amino acid) orexin/hypocretin peptide	Phoenix, rabbit polyclonal, cat.# G- 003–30; lot# 01282–3; RRID: AB_2315019	1:5,000
Tyrosine hydroxylase (TH)	Denatured tyrosine hydroxylase from rat pheochromocytoma (denatured by sodium dodecyl sulfate).	Millipore, rabbit polyclonal, cat. #AB152, lot# 240602, RRID: AB_696697	1:10,000

Table 3.

Co-localization of mRNA and protein in Syp-mCherry-expressing neurons

Vglut2 case #	**Syp-mCherry**	***Slc17a6* mRNA**	**Percent co-localization**
1280	512	510	99.6%
1281	674	674	100.0%
Total	**1186**	**1184**	**99.8%**
FoxP2 case #	**Syp-mCherry**	**FoxP2 nuclear immunoreactivity**	**Percent co-localization**
1404	194	190	97.9%
1405	135	134	99.3%
Total	**329**	**324**	**98.5%**
Pdyn case #	**Syp-mCherry**	**FoxP2 nuclear immunoreactivity**	**Percent co-localization**
1812	93	87	93.5%
1814	85	72	84.7%
Total	**178**	**159**	**89.3%**
Pdyn case #	**Syp-mCherry**	***Pdyn* mRNA**	**Percent co-localization**
1812	70	69	98.6%
1813	37	37	100.0%
1814	128	127	99.2%
Total	**235**	**233**	**99.1%**